



**HAL**  
open science

# MLLA INCLUSIVE HADRONIC DISTRIBUTIONS INSIDE ONE JET AT HIGH ENERGY COLLIDERS

Redamy Perez Ramos, Bruno Machet

► **To cite this version:**

Redamy Perez Ramos, Bruno Machet. MLLA INCLUSIVE HADRONIC DISTRIBUTIONS INSIDE ONE JET AT HIGH ENERGY COLLIDERS. 2006. hal-00016106v2

**HAL Id: hal-00016106**

**<https://hal.science/hal-00016106v2>**

Preprint submitted on 10 Jan 2006 (v2), last revised 7 Apr 2006 (v4)

**HAL** is a multi-disciplinary open access archive for the deposit and dissemination of scientific research documents, whether they are published or not. The documents may come from teaching and research institutions in France or abroad, or from public or private research centers.

L'archive ouverte pluridisciplinaire **HAL**, est destinée au dépôt et à la diffusion de documents scientifiques de niveau recherche, publiés ou non, émanant des établissements d'enseignement et de recherche français ou étrangers, des laboratoires publics ou privés.

January 2006

## MLLA INCLUSIVE HADRONIC DISTRIBUTIONS INSIDE ONE JET AT HIGH ENERGY COLLIDERS

R. Perez-Ramos <sup>1</sup> & B. Machet <sup>2</sup>

*Laboratoire de Physique Théorique et Hautes Energies <sup>3</sup>*  
*UMR 7589, CNRS et Universités Paris 6 et Paris 7*

**Abstract:** After demonstrating their general expressions valid at all  $x$ , double differential 1-particle inclusive distributions inside a quark and a gluon jet produced in a hard process, together with the inclusive  $k_{\perp}$  distributions, are calculated at small  $x$  in the Modified Leading Logarithmic Approximation (MLLA), as functions of the transverse momentum  $k_{\perp}$  of the outgoing hadron. Results are compared with the Double Logarithmic Approximation (DLA) and a naive DLA-inspired evaluation.

*Keywords: perturbative Quantum Chromodynamics, jets, high-energy colliders*



---

<sup>1</sup>E-mail: perez@lpthe.jussieu.fr

<sup>2</sup>E-mail: machet@lpthe.jussieu.fr

<sup>3</sup>LPTHE, tour 24-25, 5<sup>ème</sup> étage, Université P. et M. Curie, BP 126, 4 place Jussieu, F-75252 Paris Cedex 05 (France)

# 1 INTRODUCTION

In high energy collisions, perturbative Quantum Chromodynamics (pQCD) successfully predicts inclusive energy spectra of particles in jets. They have been determined within the Modified Leading Logarithmic Approximation (MLLA) [1] [2] as functions of the logarithm of the energy ( $\ln(1/x)$ ) and the result is in nice agreement with the data of  $e^+e^-$  and hadronic colliders and of deep inelastic scattering (DIS) (see for example [3] [4] [5]). Though theoretical predictions have been derived for small  $x$  (energy fraction of one parton inside the jet,  $x \ll 1$ )<sup>4</sup>, the agreement turns out to hold even for  $x \sim 1$ . The infrared transverse momentum cutoff  $Q_0$  can even be set as low as the intrinsic QCD scale  $\Lambda_{QCD}$  (the so-called “limiting spectrum”).

This work concerns the production of two hadrons inside a high energy jet (quark or gluon); more specifically, we study, in the MLLA scheme of resummation, the double differential inclusive 1-particle distribution and the inclusive  $k_\perp$  distribution as functions of the transverse momentum of the emitted hadrons.

While in  $e^+e^-$  colliders, no interference between ingoing states (leptons) and outgoing hadrons occurs, the situation is different in hadronic colliders; to avoid them, one must consider small jet cones.

Up to now, this type of process has only been investigated in the DLA approximation [1].

The plan of the paper is the following:

- The description of the process, the notations and conventions are presented in section 2. We set there the general formula of the inclusive 2-particle differential cross section for the production of two hadrons  $h_1$  and  $h_2$  at angle  $\Theta$  within a jet of opening angle  $\Theta_0$ , carrying respectively the fractions  $x_1$  and  $x_2$  of the jet energy  $E$ ; the axis of the jet is identified with the direction of the energy flow.
- In section 3, we determine the double differential inclusive 1-particle distribution  $\frac{d^2N}{d\ln(1/x_1)d\ln\Theta}$  for the hadron  $h_1$  emitted with the energy fraction  $x_1$  of the jet energy  $E$ , at an angle  $\Theta$  with respect to the jet axis. This expression is valid for all  $x$ ; it however only simplifies for  $x \ll 1$ , where an analytical expression can be obtained; this concerns the rest of the paper.
- In section 4, we go to the small  $x$  region and determine  $\frac{d^2N}{d\ln(1/x_1)d\ln\Theta}$ ,  $x_1 \ll 1$  both for a gluon jet and for a quark jet. It is plotted as a function of  $\ln k_\perp$  (or  $\ln \Theta$ ) for different values of  $\ell_1 = \ln(1/x_1)$ ; the role of the opening angle  $\Theta_0$  of the jet is also considered; we compare in particular the MLLA calculation [6] with a naive approach, inspired by DLA calculations, in which furthermore the evolution of the jet is not taken into account.
- In section 5, we study the inclusive  $k_\perp$  distribution  $\frac{dN}{d\ln k_\perp}$ , which is the integral of  $\frac{d^2N}{dx_1 d\ln\Theta}$  with respect to  $x_1$ . The case of mixed gluon and quark jets is evoked.
- A conclusion summarizes the results of this work.

Five appendices complete this work; the first four provide detailed derivations of the formulæ displayed in the core of the paper; the fifth is dedicated to a comparison between MLLA and DLA calculations.

---

<sup>4</sup>as the exact solution of the MLLA Evolution Equations

- Appendix A is dedicated to the MLLA evolution equation for the partonic fragmentation functions  $D_g^{g \text{ or } q}$  and their exact solutions [6]. They are plotted, together with their derivatives with respect to  $\ln(1/x)$  and  $\ln k_\perp$ . This eases the understanding of the figures in the core of the paper and shows the consistency of our calculations.
- Appendix B presents the explicit expressions at leading order for the average color currents of partons  $\langle C \rangle_{A_0}$ .
- Appendix C completes section 4 by providing explicit formulæ necessary for the calculation of  $\frac{d^2 N}{dx_1 d \ln \Theta}$  at small  $x_1$ ;
- in Appendix D, we compare the leading and MLLA expressions of the average gluon and quark color currents  $\langle C \rangle_g$  and  $\langle C \rangle_q$  defined in section 4;
- in Appendix E, we compare the DLA and MLLA approximations for the spectrum, the double differential 1-particle inclusive distribution, and the inclusive  $k_\perp$  distribution.

## 2 THE PROCESS UNDER CONSIDERATION

It is depicted in Fig. 1 below. In a hard collision, a parton  $A_0$  is produced, which can be a quark or a gluon<sup>5</sup>.  $A_0$ , by a succession of partonic emissions (quarks, gluons), produces a jet of opening angle  $\Theta_0$ , which, in particular, contains the parton  $A$ ;  $A$  splits into  $B$  and  $C$ , which hadronize respectively into the two hadrons  $h_1$  and  $h_2$  (and other hadrons).  $\Theta$  is the angle between  $B$  and  $C$ .

Because the virtualities of  $B$  and  $C$  are much smaller than that of  $A$  [7],  $\Theta$  can be considered to be close to the angle between  $h_1$  and  $h_2$  [7][8]; angular ordering is also a necessary condition for this property to hold.

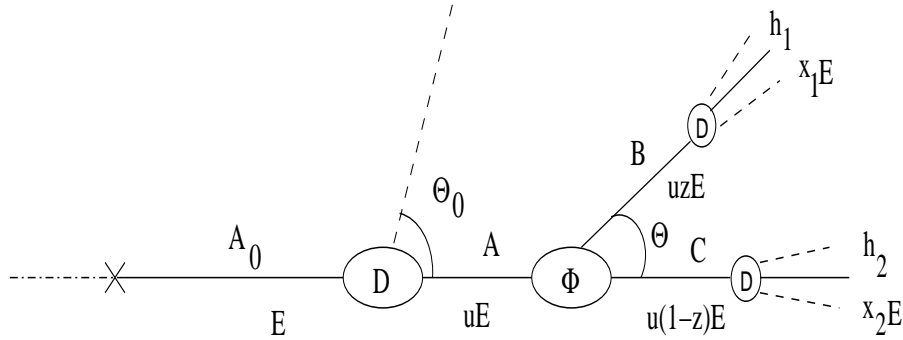


Fig. 1: process under consideration: two hadrons  $h_1$  and  $h_2$  inside one jet.

$A_0$  carries the energy  $E$ . With a probability  $D_{A_0}^A$ , it gives rise to the (virtual) parton  $A$ , which carries the fraction  $u$  of the energy  $E$ ;  $\Phi_A^{BC}(z)$  is the splitting function of  $A$  into  $B$  and  $C$ , carrying respectively

<sup>5</sup>in  $p-p$  or  $p-\bar{p}$  collisions, two partons collide which can create  $A_0$  either as a quark or as a gluon; in the deep inelastic scattering (DIS) and in  $e^+e^-$  colliders, a vector boson ( $\gamma$  or  $Z$ ) decays into a quark-antiquark pair, and  $A_0$  is a quark (or an antiquark);

the fractions  $uz$  and  $u(1-z)$  of  $E$ ;  $h_1$  carries the fraction  $x_1$  of  $E$ ;  $h_2$  carries the fraction  $x_2$  of  $E$ ;  $D_B^{h_1} \left( \frac{x_1}{uz}, uzE\Theta, Q_0 \right)$  and  $D_C^{h_2} \left( \frac{x_2}{u(1-z)}, u(1-z)E\Theta, Q_0 \right)$  are their respective energy distributions. One has  $\Theta \leq \Theta_0$ . On the other hand, since  $k_\perp \geq Q_0$  ( $Q_0$  is the collinear cutoff), the emission angle must satisfy  $\Theta \geq \Theta_{min} = Q_0/(xE)$ ,  $x$  being the fraction of the energy  $E$  carried away by this particle (see also subsection 2.1 below).

The following expression for the inclusive double differential 2-particle cross section has been demonstrated in [7] [8]:

$$\frac{d\sigma}{d\Omega_{jet} dx_1 dx_2 d \ln \left( \sin^2 \frac{\Theta}{2} \right) \frac{d\varphi}{2\pi}} = \left( \frac{d\sigma}{d\Omega_{jet}} \right)_0 \sum_{A,B,C} \int \frac{du}{u^2} \int \frac{dz}{z(1-z)} \frac{\alpha_s(k_\perp^2)}{4\pi} \Phi_A^{BC}(z) D_{A_0}^A(u, E\Theta_0, uE\Theta) D_B^{h_1} \left( \frac{x_1}{uz}, uzE\Theta, Q_0 \right) D_C^{h_2} \left( \frac{x_2}{u(1-z)}, u(1-z)E\Theta, Q_0 \right), \quad (1)$$

where  $\left( \frac{d\sigma}{d\Omega_{jet}} \right)_0$  is the Born cross section for the production of  $A_0$ ,  $\Omega_{jet}$  is the solid angle of the jet and  $\varphi$  is the azimuthal angle between  $B$  and  $C$ .

$\alpha_s(q^2)$  is the QCD running coupling constant:

$$\alpha_s(q^2) = \frac{4\pi}{4N_c \beta \ln \frac{q^2}{\Lambda_{QCD}^2}}, \quad (2)$$

where  $\Lambda_{QCD} \approx$  a few hundred  $MeV$  is the intrinsic scale of QCD and

$$\beta = \frac{1}{4N_c} \left( \frac{11}{3} N_c - \frac{4}{3} T_R \right) \quad (3)$$

is the first term in the perturbative expansion of the  $\beta$ -function,  $N_c$  is the number of colors,  $T_R = n_f/2$ , where  $n_f$  is the number of light quark flavors ( $n_f = 3$ ); it is convenient to scale all relevant parameters in units of  $4N_c$ .

In (1), the integrations over  $u$  and  $z$  are performed from 0 to 1; the appropriate step functions ensuring  $uz \geq x_1$ ,  $u(1-z) \geq x_2$  (positivity of energy) are included in  $D_B^{h_1}$  and  $D_C^{h_2}$ .

## 2.1 Notations and variables

The notations and conventions, that are used above and throughout the paper are the following. For any given particle with 4-momentum  $(k_0, \vec{k})$ , transverse momentum  $k_\perp \geq Q_0$  ( $k_\perp$  is the modulus of the trivector  $\vec{k}_\perp$ ), carrying the fraction  $x = k_0/E$  of the jet energy  $E$ , one defines

$$\ell = \ln \frac{E}{k_0} = \ln(1/x), \quad y = \ln \frac{k_\perp}{Q_0}. \quad (4)$$

$Q_0$  is the infrared cutoff parameter (minimal transverse momentum).

If the radiated parton is emitted with an angle  $\vartheta$  with respect to the direction of the jet, one has

$$k_\perp = |\vec{k}| \sin \vartheta \approx k_0 \sin \vartheta. \quad (5)$$

The r.h.s. of (5) uses  $|\vec{k}| \approx k_0$ , resulting from the property that the virtuality  $k^2$  of the emitted parton is negligible in the logarithmic approximation.

For collinear emissions ( $\vartheta \ll 1$ ),  $k_\perp \sim |\vec{k}|\vartheta \approx k_0\vartheta$ .

One also defines the variable  $Y_\vartheta$

$$Y_\vartheta = \ell + y = \ln \left( E \frac{k_\perp}{k_0} \frac{1}{Q_0} \right) \approx \ln \frac{E\vartheta}{Q_0}; \quad (6)$$

to the opening angle  $\Theta_0$  of the jet corresponds

$$Y_{\Theta_0} = \ln \frac{E\Theta_0}{Q_0}. \quad (7)$$

$E\Theta_0$  measures the ‘‘hardness’’ of the jet.

Since  $\vartheta < \Theta_0$ , one has the condition, valid for any emitted soft parton off its ‘‘parent’’

$$Y_\vartheta < Y_{\Theta_0}. \quad (8)$$

The partonic fragmentation function  $D_a^b(x_b, Q, q)$  represents the probability of finding the parton  $b$  having the fraction  $x_b$  of the energy of  $a$  inside the dressed parton  $a$ ; the virtuality (or transverse momentum)  $k_a^2$  of  $a$  can go up to  $|Q^2|$ , that of  $b$  can go down to  $|q^2|$ .

## 2.2 The jet axis

The two quantities studied in the following paragraphs (double differential 1-particle inclusive distribution and inclusive  $k_\perp$  distribution) refer to the direction (axis) of the jet, with respect to which the angles are measured. We identify it with the direction of the energy flow.

The double differential 1-particle inclusive distribution  $\frac{d^2N}{dx_1 d \ln \Theta}$  is accordingly defined by summing the inclusive double differential 2-particle cross section over all  $h_2$  hadrons and integrating it over their energy fraction  $x_2$  with a weight which is the energy ( $x_2$ ) itself; it measures the angular distribution of an outgoing hadron  $h_1$  with energy fraction  $x_1$  of the jet energy, produced at an angle  $\Theta$  with respect to the direction of the energy flow.

Once the axis has been fixed, a second (unweighted) integration with respect to the energy of the other hadron ( $x_1$ ) leads to the inclusive  $k_\perp$  distribution  $\frac{dN}{d \ln k_\perp}$ .

## 3 DOUBLE DIFFERENTIAL 1-PARTICLE INCLUSIVE DISTRIBUTION $\frac{d^2N}{dx_1 d \ln \Theta}$

After integrating trivially over the azimuthal angle (at this approximation the cross-section does not depend on it), and going to small  $\Theta$ , the positive quantity  $\frac{d^2N}{dx_1 d \ln \Theta}$  reads

$$\frac{d^2N}{dx_1 d \ln \Theta} = \sum_{h_2} \int_0^1 dx_2 x_2 \frac{d\sigma}{d\Omega_{jet} dx_1 dx_2 d \ln \Theta} \frac{1}{\left( \frac{d\sigma}{d\Omega_{jet}} \right)_0}. \quad (9)$$

We use the energy conservation sum rule [9]

$$\sum_h \int_0^1 dx x D_C^h(x, \dots) = 1 \quad (10)$$

expressing that all partons  $h_2$  within a dressed parton ( $C$ ) carry the total momentum of  $C$ , then make the change of variable  $v = \frac{x}{u(1-z)}$  where  $u(1-z)$  is the upper kinematic limit for  $x_2$ , to get

$$\sum_{h_2} \int_0^{u(1-z)} dx_2 x_2 D_C^{h_2} \left( \frac{x_2}{u(1-z)}, u(1-z)E\Theta, Q_0 \right) = u^2(1-z)^2, \quad (11)$$

and finally obtain the desired quantity;

$$\frac{d^2 N}{dx_1 d \ln \Theta} = \sum_{A,B} \int du \int dz \frac{1-z}{z} \frac{\alpha_s(k_\perp^2)}{2\pi} \Phi_A^B(z) D_{A_0}^A(u, E\Theta_0, uE\Theta) D_B^{h_1} \left( \frac{x_1}{uz}, uzE\Theta, Q_0 \right); \quad (12)$$

the summation index  $C$  has been suppressed since knowing  $A$  and  $B$  fixes  $C$ .

We can transform (12) by using the following trick:

$$\int du \int \frac{dz}{z} (1-z) = \int du \int \frac{dz}{z} - \int d(uz) \int \frac{du}{u}, \quad (13)$$

and (12) becomes

$$\begin{aligned} \frac{d^2 N}{dx_1 d \ln \Theta} &= \sum_A \int du D_{A_0}^A(u, E\Theta_0, uE\Theta) \sum_B \int \frac{dz}{z} \frac{\alpha_s(k_\perp^2)}{2\pi} \Phi_A^B(z) D_B^{h_1} \left( \frac{x_1}{uz}, uzE\Theta, Q_0 \right) \\ &\quad - \sum_B \int d(uz) D_B^{h_1} \left( \frac{x_1}{uz}, uzE\Theta, Q_0 \right) \sum_A \int \frac{du}{u} \frac{\alpha_s(k_\perp^2)}{4\pi} \Phi_A^B \left( \frac{uz}{u} \right) D_{A_0}^A(u, E\Theta_0, uE\Theta). \end{aligned} \quad (14)$$

We then make use of the two complementary DGLAP (see also the beginning of section 4) evolution equations [10] which contain the Sudakov form factors  $d_A$  and  $d_B$  of the partons  $A$  and  $B$  respectively:

$$d_A^{-1}(k_A^2) \frac{d}{d \ln k_A^2} \left[ d_A(k_A^2) D_A^{h_1} \left( \frac{x_1}{u}, uE\Theta, Q_0 \right) \right] = \frac{\alpha_s(k_\perp^2)}{4\pi} \sum_B \int \frac{dz}{z} \Phi_A^B(z) D_B^{h_1} \left( \frac{x_1}{uz}, uzE\Theta, Q_0 \right), \quad (15)$$

$$d_B(k_B^2) \frac{d}{d \ln k_B^2} \left[ d_B^{-1}(k_B^2) D_{A_0}^B(uz, E\Theta_0, uE\Theta) \right] = -\frac{\alpha_s(k_\perp^2)}{4\pi} \sum_A \int \frac{du}{u} \Phi_A^B \left( \frac{uz}{u} \right) D_{A_0}^A(u, E\Theta_0, uE\Theta); \quad (16)$$

the variable  $uz$  occurring in (13) has been introduced; in (15) and (16),  $(uE\Theta)^2$  refers respectively to the virtualities  $k_A^2$  and  $k_B^2$  of  $A$  and  $B$ .

Using (15) and (16), (14) transforms into

$$\begin{aligned} \frac{d^2 N}{dx_1 d \ln \Theta} &= \sum_A \int du D_{A_0}^A(u, E\Theta_0, uE\Theta) d_A^{-1}(k_A^2) \frac{d}{d \ln k_A^2} \left[ d_A(k_A^2) D_A^{h_1} \left( \frac{x_1}{u}, uE\Theta, Q_0 \right) \right] \\ &\quad + \sum_B \int d(uz) D_B^{h_1} \left( \frac{x_1}{uz}, uzE\Theta, Q_0 \right) d_B(k_B^2) \frac{d}{d \ln k_B^2} \left[ d_B^{-1}(k_B^2) D_{A_0}^B(uz, E\Theta_0, uE\Theta) \right]. \end{aligned} \quad (17)$$

$D_A^{h_1}$  depends on the virtuality of  $A$  through the variable [1]  $\Delta\xi = \xi(k_A^2) - \xi(Q_0^2) = \frac{1}{4N_c\beta} \ln \left( \frac{\ln(k_A^2/\Lambda_{QCD}^2)}{\ln(Q_0^2/\Lambda_{QCD}^2)} \right)$

and elementary kinematic considerations [7] lead to  $k_A^2 \sim (uE\Theta)^2$ .

By renaming  $B \rightarrow A$  and  $uz \rightarrow u$ , (17) finally becomes

$$\begin{aligned} \frac{d^2 N}{dx_1 d \ln \Theta} &= \sum_A \int du \left[ D_{A_0}^A(u, E\Theta_0, uE\Theta) d_A^{-1}(k_A^2) \frac{d}{d \ln \Theta} \left[ d_A(k_A^2) D_A^{h_1} \left( \frac{x_1}{u}, uE\Theta, Q_0 \right) \right] \right. \\ &\quad \left. + D_A^{h_1} \left( \frac{x_1}{u}, uE\Theta, Q_0 \right) d_A(k_A^2) \frac{d}{d \ln \Theta} \left[ d_A^{-1}(k_A^2) D_{A_0}^A(u, E\Theta_0, uE\Theta) \right] \right] \\ &= \sum_A \frac{d}{d \ln \Theta} \left[ \int du D_{A_0}^A(u, E\Theta_0, uE\Theta) D_A^{h_1} \left( \frac{x_1}{u}, uE\Theta, Q_0 \right) \right], \end{aligned} \quad (18)$$

and one gets

$$\frac{d^2 N}{dx_1 d \ln \Theta} = \frac{d}{d \ln \Theta} F_{A_0}^{h_1}(x_1, \Theta, E, \Theta_0) \quad (19)$$

with

$$F_{A_0}^{h_1}(x_1, \Theta, E, \Theta_0) \equiv \sum_A \int du D_{A_0}^A(u, E\Theta_0, uE\Theta) D_A^{h_1} \left( \frac{x_1}{u}, uE\Theta, Q_0 \right); \quad (20)$$

$F$  defined in (20) is the inclusive double differential distribution in  $x_1$  and  $\Theta$  with respect to the energy flux (the energy fraction of the hadron  $h_1$  within the registered energy flux) and is represented by the convolution of the two functions  $D_{A_0}^A$  and  $D_A^h$ .

The general formula (19) is valid for all  $x_1$ ; its analytical expression in the small  $x_1$  region will be written in the next section.

## 4 SOFT APPROXIMATION (SMALL- $x_1$ ) FOR $\frac{d^2 N}{d\ell_1 d \ln k_\perp}$

At  $\ell_1$  fixed, since  $y_1 = \ln(k_\perp/Q_0)$  and  $Y = \ln(E\Theta/Q_0) = \ell_1 + y_1$ ,  $dy_1 = d \ln k_\perp = d \ln \Theta$  and we write hereafter  $\frac{d^2 N}{d\ell_1 d \ln k_\perp}$  or  $\frac{d^2 N}{d\ell_1 dy_1}$  instead of  $\frac{d^2 N}{d\ell_1 d \ln \Theta}$ .

Since the  $u$ -integral (20) is dominated by  $u = \mathcal{O}(1)$ <sup>6</sup>, the DGLAP [1] partonic distributions  $D_{A_0}^A(u, \dots)$  are to be used and, since, on the other hand, we restrict to small  $x_1$ ,  $x_1/u \ll 1$  and the MLLA inclusive  $D_A^{h_1}((x_1/u), \dots)$  are requested. The latter will be taken as the exact solution of the (MLLA) evolution equations that are demonstrated in [6] and that we briefly recall, for the sake of completeness, in appendix A. MLLA evolution equations accounts for the constraints of angular ordering (like DLA but unlike DGLAP equations) and of energy-momentum conservation (unlike DLA).

For soft hadrons, the behavior of the function  $D_A^{h_1}(x_1, E\Theta, Q_0)$  at  $x_1 \ll 1$  is [1]

$$D_A^{h_1}(x_1, E\Theta, Q_0) \approx \frac{1}{x_1} \rho_A^{h_1} \left( \ln \frac{1}{x_1}, \ln \frac{E\Theta}{Q_0} \equiv Y_\Theta \right), \quad (21)$$

---

<sup>6</sup> $D_A^{h_1} \left( \frac{x_1}{u}, uE\Theta, Q_0 \right) \approx (u/x_1) \times$  (slowly varying function) – see (22) – and the most singular possible behavior of  $D_{A_0}^A(u, E\Theta_0, uE\Theta, Q_0)$ , which could enhance the contribution of small  $u$ , is  $\sim 1/u$ ; however, the integrand then behaves like  $\text{Const.} \times$  (slowly varying function) and the contribution of small  $u$  to the integral is still negligible.



where  $\rho_A^{h_1}$  is a slowly varying function of two logarithmic variables that describes the ‘‘hump-backed’’ plateau.

For  $D_A^{h_1}\left(\frac{x_1}{u}, uE\Theta, Q_0\right)$  occurring in (20), this yields

$$D_A^{h_1}\left(\frac{x_1}{u}, uE\Theta, Q_0\right) \approx \frac{u}{x_1} \rho_A^{h_1}\left(\ln \frac{u}{x_1}, \ln u + Y_\Theta\right). \quad (22)$$

Because of (6), one has

$$\rho_A^h(\ell, Y_\Theta) = \rho_A^{h_1}(\ell, \ell + y) = \tilde{D}_A^h(\ell, y), \quad (23)$$

and, in what follows, we shall always consider the functions

$$xD_A(x, E\Theta, Q_0) = \tilde{D}_A(\ell, y). \quad (24)$$

The expansion of  $\rho_A^{h_1}\left(\ln \frac{u}{x_1}, \ln u + Y_\Theta\right)$  around  $u = 1$  ( $\ln u = \ln 1$ ) reads

$$\begin{aligned} \frac{x_1}{u} D_A^{h_1}\left(\frac{x_1}{u}, uE\Theta, Q_0\right) &= \rho_A^{h_1}(\ell_1 + \ln u, Y_\Theta + \ln u) = \rho_A^{h_1}(\ell_1 + \ln u, y_1 + \ell_1 + \ln u) \\ &= \tilde{D}_A^{h_1}(\ell_1 + \ln u, y_1) = \tilde{D}_A^{h_1}(\ell_1, y_1) + \ln u \frac{d}{d\ell_1} \tilde{D}_A^{h_1}(\ell_1, y_1) + \dots, \end{aligned} \quad (25)$$

such that

$$\begin{aligned} x_1 F_{A_0}^{h_1}(x_1, \Theta, E, \Theta_0) &\approx \sum_A \int du u D_{A_0}^A(u, E\Theta_0, uE\Theta) \left( \tilde{D}_A^{h_1}(\ell_1, y_1) + \ln u \frac{d\tilde{D}_A^{h_1}(\ell_1, y_1)}{d\ell_1} \right) \\ &= \sum_A \left[ \int du u D_{A_0}^A(u, E\Theta_0, uE\Theta) \right] \tilde{D}_A^{h_1}(\ell_1, y_1) \\ &\quad + \sum_A \left[ \int du u \ln u D_{A_0}^A(u, E\Theta_0, uE\Theta) \right] \frac{d\tilde{D}_A^{h_1}(\ell_1, y_1)}{d\ell_1}; \end{aligned} \quad (26)$$

the second line in (26) is the  $\mathcal{O}(\sqrt{\alpha_s})$  main contribution, the third line, which accounts for the derivatives, including the variation of  $\alpha_s$ , makes up corrections of relative order  $\mathcal{O}(\sqrt{\alpha_s})$  with respect to the leading terms (see also (37)).

It is important for further calculations that (20) has now factorized.

While (20) (26) involve (inclusive) *hadronic* fragmentation functions  $\tilde{D}_A^{h_1} = \tilde{D}_g^{h_1}$  or  $\tilde{D}_q^{h_1}$ , the MLLA *partonic* functions  $\tilde{D}_A^b(\ell, y)$  satisfy the evolution equations (45) with exact solution (51), demonstrated in [6] and recalled in appendix A. The link between the latter ( $\tilde{D}_g^g, \tilde{D}_q^g, \tilde{D}_g^q, \tilde{D}_q^q$ ) and the former goes as follows. At small  $x$ , since quarks are secondary products of gluons, for a given ‘‘parent’’, the number of emitted quarks is a universal function of the number of emitted gluons: the upper indices of emitted partons are thus correlated, and we can replace in (26) the inclusive fragmentation functions by the partonic ones, go to the functions  $\tilde{D}_A(\ell, y)$ , where the upper index (which we will omit) is indifferently  $g$  or  $q$ , and rewrite

$$x_1 F_{A_0}^{h_1}(x_1, \Theta, E, \Theta_0) \approx \sum_A \left( \langle u \rangle_{A_0}^A + \delta \langle u \rangle_{A_0}^A \psi_{A, \ell_1}(\ell_1, y_1) \right) \tilde{D}_A(\ell_1, y_1), \quad (27)$$

with <sup>7</sup>

$$\langle u \rangle_{A_0}^A = \int_0^1 du u D_{A_0}^A(u, E\Theta_0, uE\Theta) \approx \int_0^1 du u D_{A_0}^A(u, E\Theta_0, E\Theta),$$

<sup>7</sup>In (28),  $u$  is integrated from 0 to 1, while, kinematically, it cannot get lower than  $x_1$ ; since we are working at small  $x_1$ , this approximation is reasonable.

$$\delta \langle u \rangle_{A_0}^A = \int_0^1 du (u \ln u) D_{A_0}^A(u, E\Theta_0, uE\Theta) \approx \int_0^1 du (u \ln u) D_{A_0}^A(u, E\Theta_0, E\Theta), \quad (28)$$

and

$$\psi_{A,\ell_1}(\ell_1, y_1) = \frac{1}{\tilde{D}_A(\ell_1, y_1)} \frac{d\tilde{D}_A(\ell_1, y_1)}{d\ell_1}. \quad (29)$$

Thus, for a gluon jet

$$\begin{aligned} x_1 F_g^{h_1}(x_1, \Theta, E, \Theta_0) &\approx \langle u \rangle_g^g \tilde{D}_g(\ell_1, y_1) + \langle u \rangle_g^q \tilde{D}_q(\ell_1, y_1) \\ &+ \delta \langle u \rangle_g^g \psi_{g,\ell_1}(\ell_1, y_1) \tilde{D}_g(\ell_1, y_1) \\ &+ \delta \langle u \rangle_g^q \psi_{q,\ell_1}(\ell_1, y_1) \tilde{D}_q(\ell_1, y_1), \end{aligned} \quad (30)$$

and for a quark jet

$$\begin{aligned} x_1 F_q^{h_1}(x_1, \Theta, E, \Theta_0) &\approx \langle u \rangle_q^g \tilde{D}_g(\ell_1, y_1) + \langle u \rangle_q^q \tilde{D}_q(\ell_1, y_1) \\ &+ \delta \langle u \rangle_q^g \psi_{g,\ell_1}(\ell_1, y_1) \tilde{D}_g(\ell_1, y_1) \\ &+ \delta \langle u \rangle_q^q \psi_{q,\ell_1}(\ell_1, y_1) \tilde{D}_q(\ell_1, y_1). \end{aligned} \quad (31)$$

It turns out (see [1]) that, the MLLA correction to the formulæ

$$\tilde{D}_g^g \approx \frac{C_F}{N_c} \tilde{D}_g^g, \quad \tilde{D}_q^q \approx \frac{C_F}{N_c} \tilde{D}_q^q, \quad (32)$$

do not modify the results and we use (32) in the following.

We rewrite accordingly (30) and (31)

$$\begin{aligned} x_1 F_g^{h_1}(x_1, \Theta, E, \Theta_0) &\approx \frac{\langle C \rangle_g^0 + \delta \langle C \rangle_g}{N_c} \tilde{D}_g(\ell_1, y_1) \equiv \frac{\langle C \rangle_g}{N_c} \tilde{D}_g(\ell_1, y_1), \\ x_1 F_q^{h_1}(x_1, \Theta, E, \Theta_0) &\approx \frac{\langle C \rangle_q^0 + \delta \langle C \rangle_q}{N_c} \tilde{D}_g(\ell_1, y_1) \equiv \frac{\langle C \rangle_q}{N_c} \tilde{D}_g(\ell_1, y_1), \end{aligned} \quad (33)$$

with

$$\begin{aligned} \langle C \rangle_g^0 &= \langle u \rangle_g^g N_c + \langle u \rangle_g^q C_F, \\ \langle C \rangle_q^0 &= \langle u \rangle_q^g N_c + \langle u \rangle_q^q C_F, \end{aligned} \quad (34)$$

and where we have called

$$\begin{aligned} \delta \langle C \rangle_g &= N_c \delta \langle u \rangle_g^g \psi_{g,\ell_1}(\ell_1, y_1) + C_F \delta \langle u \rangle_g^q \psi_{q,\ell_1}(\ell_1, y_1), \\ \delta \langle C \rangle_q &= N_c \delta \langle u \rangle_q^g \psi_{g,\ell_1}(\ell_1, y_1) + C_F \delta \langle u \rangle_q^q \psi_{q,\ell_1}(\ell_1, y_1). \end{aligned} \quad (35)$$

$\langle C \rangle_{A_0}$  is the average color current of partons caught by the calorimeter.

Plugging (33) into (19) yields the general formula

$$\left( \frac{d^2 N}{d\ell_1 d \ln k_\perp} \right)_{q,g} = \frac{d}{dy_1} \left[ \frac{\langle C \rangle_{q,g}}{N_c} \tilde{D}_g(\ell_1, y_1) \right] \quad (36)$$

The first line of (30) and (31) are the leading terms, the second and third lines are corrections. Their relative order is easily determined by the following relations (see (46) for the definition of  $\gamma_0$ )

$$\begin{aligned}\frac{d^2 N}{d\ell_1 d\ln k_\perp} &= \frac{\langle C \rangle_{q,g}}{N_c} \frac{d}{dy_1} \tilde{D}_g(\ell_1, y_1) + \frac{1}{N_c} \tilde{D}_g(\ell_1, y_1) \frac{d}{dy_1} \langle C \rangle_{q,g}, \\ \frac{d}{dy_1} \tilde{D}_g(\ell_1, y_1) &= \mathcal{O}(\gamma_0) = \mathcal{O}(\sqrt{\alpha_s}), \\ \frac{d}{dy_1} \langle C \rangle_{q,g} &= \mathcal{O}(\gamma_0^2) = \mathcal{O}(\alpha_s);\end{aligned}\tag{37}$$

the third line of (37), which corresponds to MLLA corrections, is  $\mathcal{O}(\sqrt{\alpha_s})$  with respect to the leading terms  $\mathcal{O}(\alpha_s)$  of the second line.

The term in (36) proportional to  $\frac{d\langle C \rangle_{A_0}}{dy}$  brings positive corrections to the leading terms in the domain of interest  $y \geq 1.4$  (see appendix D).

•  $\frac{d\tilde{D}_g(\ell, y)}{d\ln k_\perp} \equiv \frac{d\tilde{D}_g(\ell, y)}{dy}$  (see the beginning of this section) occurring in (36) is plotted in Fig. 11 and 12 of appendix A, and  $\frac{d\tilde{D}_g(\ell, y)}{d\ell}$  occurring in (27) (29) is plotted in Figs. 13 and 14.

• The expressions for the leading terms of  $x_1 F_{A_0}^{h_1}(x_1, \Theta, E, \Theta_0)$  together with the ones of  $\langle C \rangle_g^0$  and  $\langle C \rangle_q^0$  are given in appendix B.

• The calculations of  $\delta \langle C \rangle_g$  and  $\delta \langle C \rangle_q$  are detailed in appendix C, where the explicit analytical expressions for the  $\langle u \rangle$ 's and  $\delta \langle u \rangle$ 's are also given.

• Graphs for  $\langle C \rangle_{A_0}$ , at leading order and including MLLA corrections, are presented in appendix D.

We call “naive” the approach” in which one disregards the evolution of the jet between  $\Theta_0$  and  $\Theta$ ; this amounts to taking to zero the derivative of  $\langle C \rangle_{q,g}$  in (36); (57), (58), (59) then yield

$$\langle C \rangle_g^{naive} = N_c, \quad \langle C \rangle_q^{naive} = C_F.\tag{38}$$

We present below our results for a gluon and for a quark jet. We choose two values  $Y_{\Theta_0} = 7.5$ , which can be associated with the LHC environment, and the unrealistic  $Y_{\Theta_0} = 10$ . For each value of  $Y_{\Theta_0}$  we make the plots for two values of  $\ell_1$ , and compare one of them with the naive approach.

In the rest of the paper we always consider the limiting case  $Q_0 \rightarrow \Lambda_{QCD} \Leftrightarrow \lambda \approx 0$ ,

$$\lambda = \ln \frac{Q_0}{\Lambda_{QCD}}.\tag{39}$$

The curves stop at their kinematic limit  $y_{1max}$  such that  $y_{1max} + \ell_1 = Y_{\Theta_0}$ .

#### 4.1 $\frac{d^2 N}{d\ell_1 d\ln k_\perp}$ at small $x_1$ : gluon jet

On Fig. 2 below is plotted the double differential distribution  $\frac{d^2 N}{d\ell_1 d\ln k_\perp}$  of a parton inside a gluon jet as a function of  $y_1$  for different values of  $\ell_1$  (fixed).

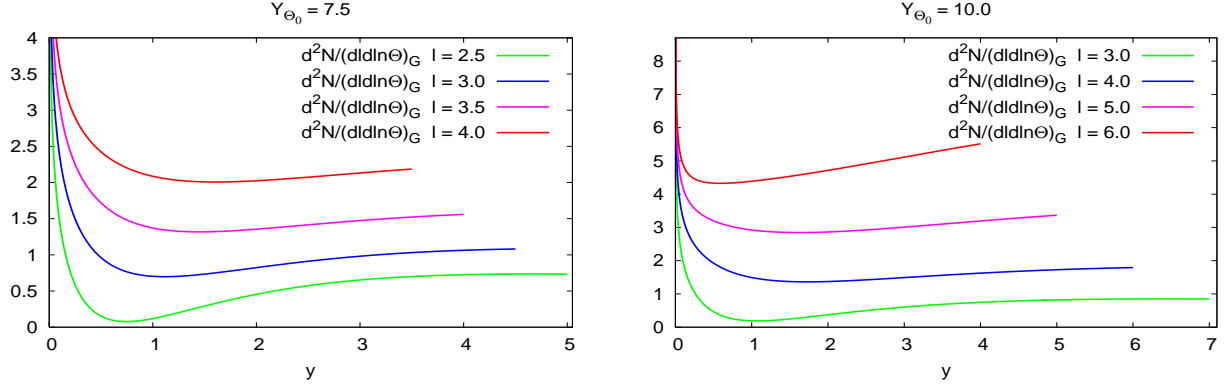


Fig. 2:  $\frac{d^2N}{d\ell_1 d\ln k_\perp}$  for a gluon jet.

On Fig. 3 are compared, for a given value of  $\ell_1$ , the two following cases:

- \* the first corresponds to the full formulæ (33) (36);
- \* the second corresponds to the naive approach (see the definition above (38))

$$\left(\frac{d^2N}{d\ell_1 d\ln k_\perp}\right)_g^{naive} = \frac{d}{dy_1} \tilde{D}_g(\ell_1, y_1); \quad (40)$$

$\frac{d\tilde{D}_g(\ell_1, y_1)}{dy_1}$  is given in (55).

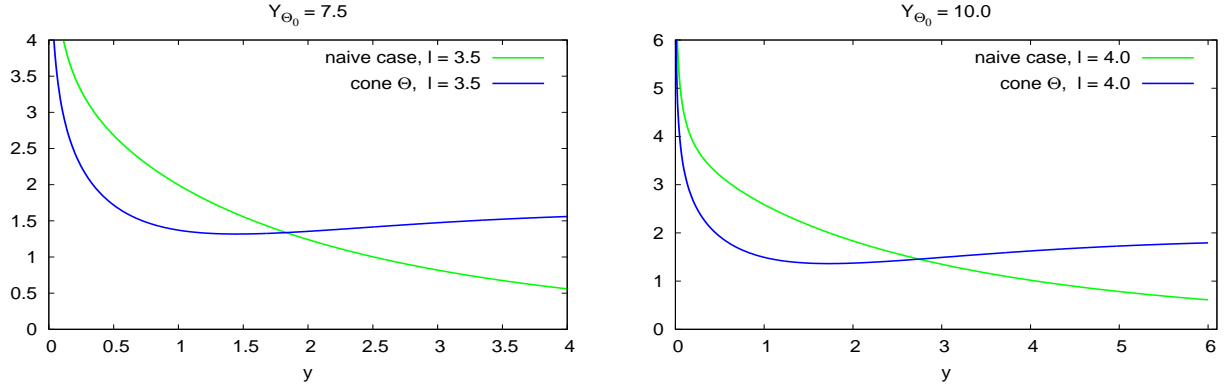


Fig. 3:  $\frac{d^2N}{d\ell_1 d\ln k_\perp}$  for a gluon jet at fixed  $\ell_1$ , MLLA and naive approach.

The raise of the distribution at large  $k_\perp$  is due to the positive corrections already mentioned in the beginning of this section, which arise from the evolution of the jet between  $\Theta$  and  $\Theta_0$ .

#### 4.2 $\frac{d^2N}{d\ell_1 d\ln k_\perp}$ at small $x_1$ : quark jet

On Fig. 4 is plotted the double differential distribution  $\frac{d^2N}{d\ell_1 d\ln k_\perp}$  of a parton inside a quark jet as a function of  $y_1$  for different values of  $\ell_1$  (fixed).

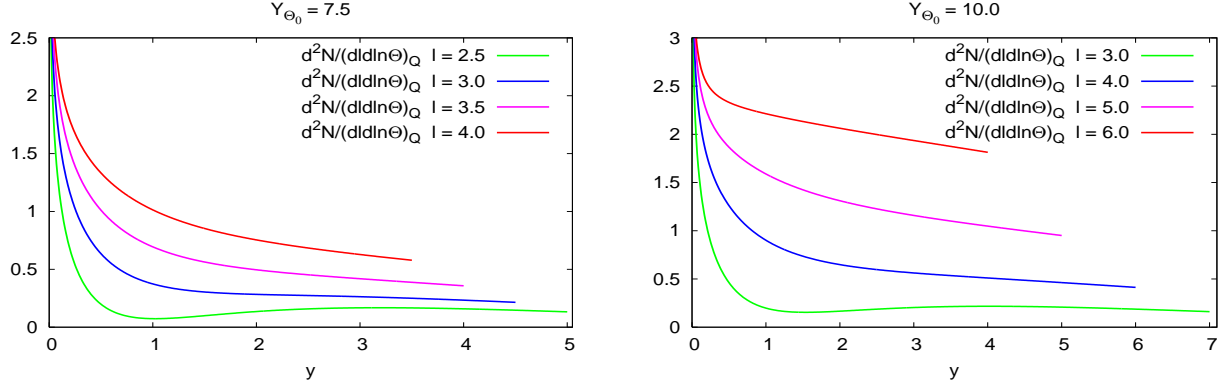


Fig. 4:  $\frac{d^2N}{d\ell_1 d\ln k_\perp}$  for a quark jet.

On Fig. 5 are compared, for a given  $\ell_1$  fixed, the full formulæ (33) (36) and the naive approach

$$\left(\frac{d^2N}{d\ell_1 d\ln k_\perp}\right)_q^{naive} = \frac{C_F}{N_c} \frac{d}{dy_1} \tilde{D}_g(\ell_1, y_1). \quad (41)$$

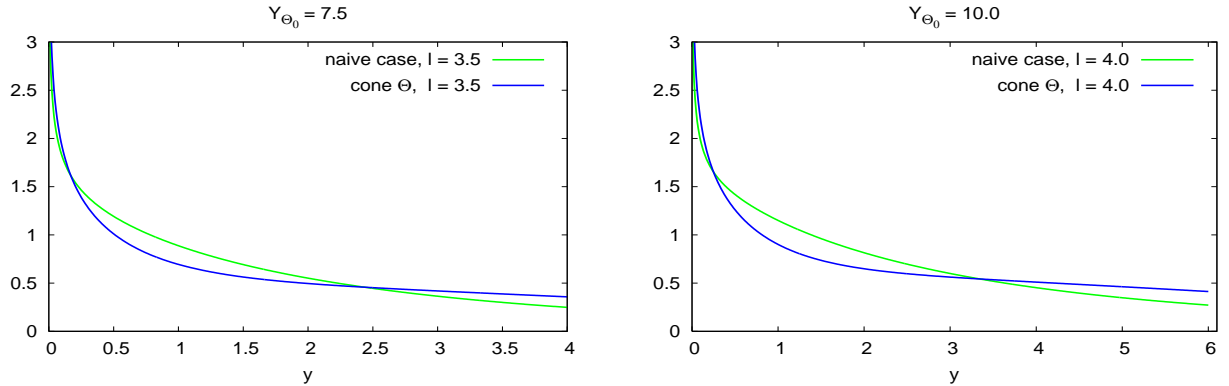


Fig. 5:  $\frac{d^2N}{d\ell_1 d\ln k_\perp}$  for a quark jet at fixed  $\ell_1$ , MLLA and naive approach.

We note, like for gluon jets, at large  $y$ , a (smaller) increase of the distribution, due to taking into account the jet evolution between  $\Theta$  and  $\Theta_0$ .

### 4.3 Comments

The curves have been drawn for values of  $\ell_1 \equiv \ln(1/x_1) \geq 1.5$  to 2; indeed, the work [6] dedicated to 2-particle correlations inside one jet in the MLLA approximation has shown that the outcome cannot be reasonably trusted for lower values of  $\ell_1$ .

Furthermore, in order to stay in the perturbative regime, one must consider  $k_\perp \geq 4Q_0 \approx 4\Lambda_{QCD} \approx 1 \text{ GeV} \Rightarrow y_1 \geq 1.4$ .

This last condition excludes in particular the zone of very large increase of  $\frac{d^2 N}{d\ell_1 d\ln k_\perp}$  when  $y_1 \rightarrow 0$  (this property is linked, in the MLLA approximation, to the divergence of the running coupling constant of QCD  $\alpha_s(k_\perp^2) \rightarrow \infty$  when  $k_\perp \rightarrow \Lambda_{QCD}$ ).

The difference between the naive and MLLA calculations lies in neglecting or not the evolution of the jet between  $\Theta_0$  and  $\Theta$ , or, in practice, in considering or not the average color current  $\langle C \rangle_{A_0}$  as a constant. MLLA corrections add a term proportional to their derivative with respect to  $y$ , the behavior of which has been plotted in Fig. 17 of appendix D; Though they can be large, specially at small values of  $\ell$ , the positivity of  $\langle C \rangle^0 + \delta \langle C \rangle$  is always preserved on the whole allowed range of  $y$ . It is expected (see [6]) that MLLA calculations cannot be reasonably trusted for  $\ell \leq 1.5 - 2$ , which roughly corresponds to the maximal values of the  $\delta \langle C \rangle$  corrections.

The gluon distribution is always larger than the quark distribution; this can also be traced in Fig. 17 which measures in particular the ratio of the color currents  $\langle C \rangle_g / \langle C \rangle_q$ .

We study in appendix E.2, how MLLA results compare with DLA [11] [12], in which the running of  $\alpha_s$  has been “subtracted”.

## 5 INCLUSIVE $k_\perp$ DISTRIBUTION $\frac{dN}{d\ln k_\perp}$

Another quantity of interest is the inclusive  $k_\perp$  distribution which is defined by

$$\left( \frac{dN}{d\ln k_\perp} \right)_{g \text{ or } q} = \int dx_1 \left( \frac{d^2 N}{dx_1 d\ln k_\perp} \right)_{g \text{ or } q} \equiv \int_{\ell_{min}}^{Y_{\Theta_0} - y} d\ell_1 \left( \frac{d^2 N}{d\ell_1 d\ln k_\perp} \right)_{g \text{ or } q}; \quad (42)$$

it measures the transverse momentum distribution of one particle with respect to the direction of the energy flow (jet axis).

We have introduced in (42) a lower bound of integration  $\ell_{min}$  because our calculations are valid for small  $x_1$ , that is for large  $\ell_1$ . In a first step we take  $\ell_{min} = 0$ , then vary it to study the sensitivity of the calculation to the region of large  $x_1$ .

We plot below the inclusive  $k_\perp$  distributions for gluon and quark jets, for the same two values  $Y_{\Theta_0} = 7.5$  and  $Y_{\Theta_0} = 10$  as above, and compare them, on the same graphs, with the “naive calculations” of the same quantity.

## 5.1 Gluon jet; $\ell_{min} = 0$

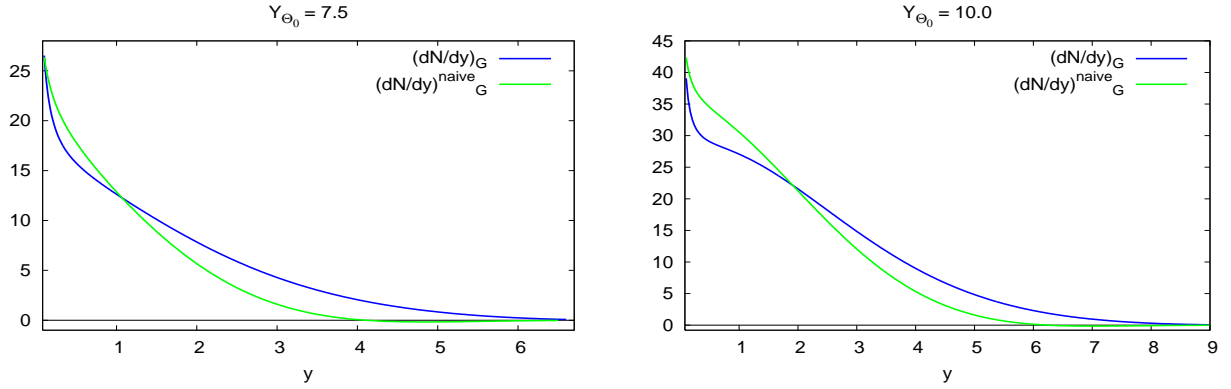


Fig. 6:  $\frac{dN}{d \ln k_{\perp}}$  for a gluon jet, MLLA and naive approach, for  $\ell_{min}=0$ ,  $Y_{\Theta_0} = 7.5$  and  $Y_{\Theta_0} = 10$ .

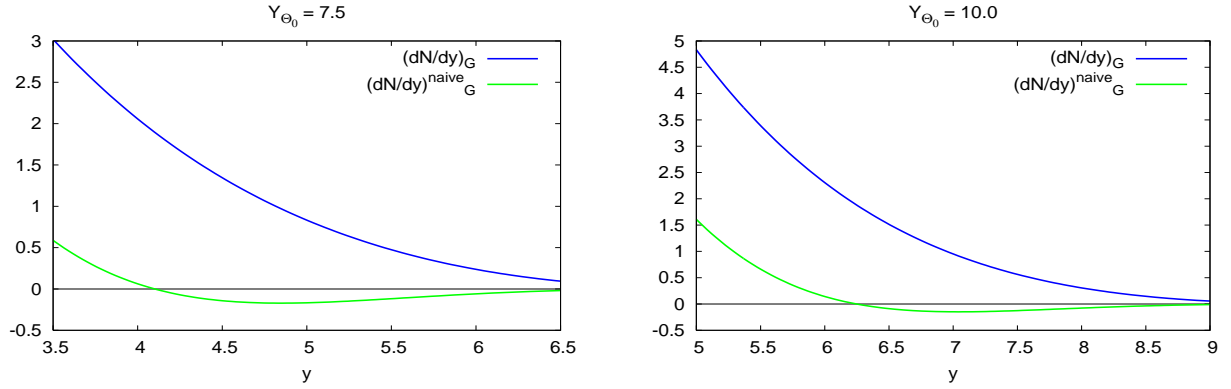


Fig. 7: enlargements of Fig. 6 at large  $k_{\perp}$

## 5.2 Quark jet; $\ell_{min} = 0$

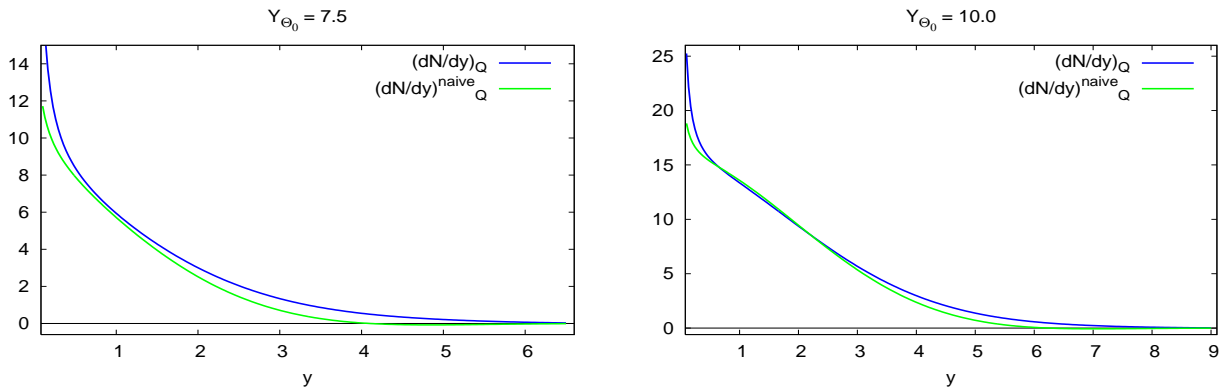


Fig. 8:  $\frac{dN}{d \ln k_{\perp}}$  for a quark jet, MLLA and naive approach, for  $\ell_{min}=0$ ,  $Y_{\Theta_0} = 7.5$  and  $Y_{\Theta_0} = 10$ .

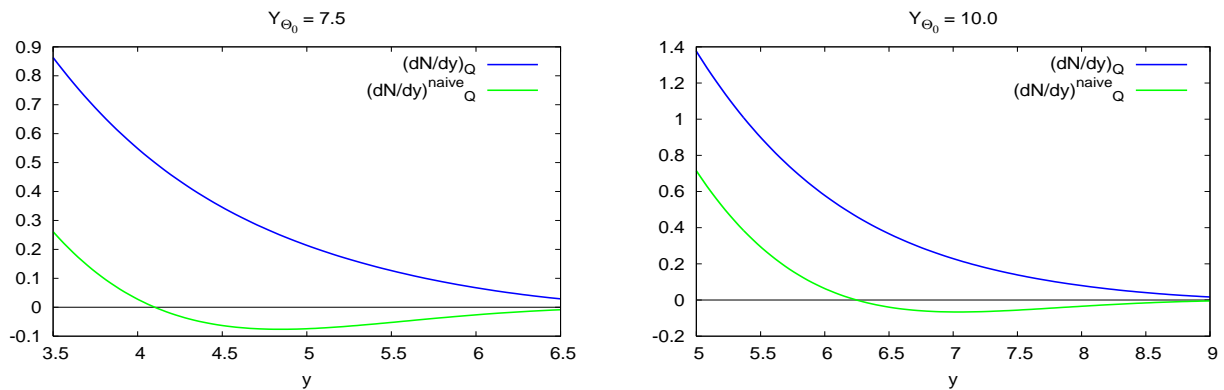


Fig. 9: enlargements of Fig. 8 at large  $k_{\perp}$

### 5.3 Role of the lower limit of integration $\ell_{min}$

To get an estimate of the sensitivity of the calculation of  $\frac{dN}{d \ln k_{\perp}}$  to the lower bound of integration in (42), we plot in Fig. 10 below the two results obtained at  $Y_{\Theta_0} = 7.5$  for  $\ell_{min} = 2$  and  $\ell_{min} = 0$ , for a gluon jet (left) and a quark jet (right).

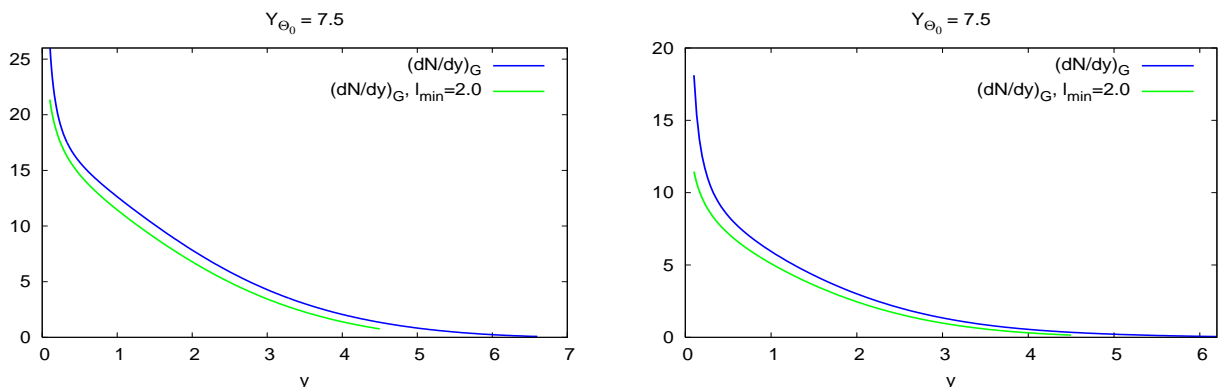


Fig. 10:  $\frac{dN}{d \ln k_{\perp}}$  with  $\ell_{min} = 2$  and  $\ell_{min} = 0$  for gluon (left) and quark (right) jet.

The shapes of the corresponding distributions are identical; they only differ by a vertical shift which is negligible in the perturbative region  $y \geq 1.5 - 2$  (restricting the domain of integration – increasing  $\ell_{min}$  – results as expected in a decrease of  $\frac{dN}{d \ln k_{\perp}}$ ). This shows that, though our calculation is only valid at small  $x_1$ , the sensitivity of the final result to this parameter is small.

### 5.4 Discussion

MLLA corrections are seen on Fig. 7 and Fig. 9 to cure the problems of positivity which occur in the naive approach.



Like the results for  $\frac{d^2N}{d\ell_1 d\ln\Theta}$ , the ones for  $\frac{dN}{d\ln k_\perp}$  can only be reasonably trusted for  $y_1 \geq 1.4$ .

On the curves of Figs. 6 and 8 at  $Y_{\Theta_0} = 10$ , the small  $y$  region exhibits a bump which comes from the competition between two phenomena: the divergence of  $\alpha_s(k_\perp^2)$  when  $k_\perp \rightarrow Q_0$  and coherence effects which deplete multiple production at very small momentum.

The separation of these two effects is still more visible at  $Y_{\Theta_0} = 15$ , which is studied in appendix E.3, where a comparison with DLA calculations is performed.

At smaller  $Y_{\Theta_0}$ , the divergence of  $\alpha_s$  wins over coherence effects and the bump disappears.

#### 5.4.1 Mixed quark and gluon jets

In many experiments, the nature of the jet (quark or gluon) is not determined, and one simply detects outgoing hadrons, which can originate from either type; one then introduces a “mixing” parameter  $\omega$ , which is to be determined experimentally, such that, for example if one deals with the inclusive  $k_\perp$  distribution

$$\left(\frac{dN}{d\ln k_\perp}\right)_{mixed} = \omega \left(\frac{dN}{d\ln k_\perp}\right)_g + (1 - \omega) \left(\frac{dN}{d\ln k_\perp}\right)_q. \quad (43)$$

It is in this framework that forthcoming data from the LHC will be compared with our theoretical predictions.

## 6 CONCLUSION

After deducing a general formula, valid for all  $x$ , for the double differential 2-particle inclusive cross section for jet production in a hard collision process, the exact solutions of the MLLA evolution equations demonstrated in [6] have been used to perform a small  $x$  calculation of the double differential 1-particle inclusive distributions and of the inclusive  $k_\perp$  distributions for quark and gluon jets.

Sizable differences with the naive approach in which one forgets the jet evolution between its opening angle  $\Theta_0$  and the emission angle  $\Theta$  have been found, in particular, the positivity of the distribution has been recovered.

The two (competing) effects of coherence (damping of multiple production at small momentum) and divergence of  $\alpha_s(k_\perp^2)$  at small  $k_\perp$  for the inclusive  $k_\perp$  distribution have been exhibited.

The “divergent” behavior of the MLLA distributions for  $y \rightarrow 0$  forbids extending the confidence domain of MLLA lower than  $y \geq 1.5$ , keeping away from the singularity of  $\alpha_s(k_\perp^2)$  when  $k_\perp \rightarrow \Lambda_{QCD}$ .

MLLA and DLA calculations have been compared; in “modified” MLLA calculations, we have furthermore canceled the  $\alpha_s$  dependence to ease the comparison with DLA.

Forthcoming data from the Tevatron and LHC will be compared with our predictions.

Further developments of this work aim at getting rid of the limit  $Q_0 \approx \Lambda_{QCD}$  and extending the calculations to a larger range of values of  $x$ ; then, because of the lack of analytical expressions, the general

formulae (19) and (20) should be numerically investigated, which will also provide a deeper insight into the connection between DGLAP and MLLA evolution equations [14].

---

*Acknowledgments:* It is a pleasure to thank M. Cacciari, Yu.L. Dokshitzer and G.P. Salam for many stimulating discussions, and for expert help in numerical calculations. R. P-R. wants to specially thank Y.L. Dokshitzer for his guidance and encouragements.

## APPENDIX

### A EXACT SOLUTION OF THE MLLA EVOLUTION EQUATION FOR THE FRAGMENTATION FUNCTIONS; THE SPECTRUM AND ITS DERIVATIVES

#### A.1 MLLA evolution equation for a gluon jet

Because of (32), we will only write the evolution equations for gluonic fragmentation functions  $D_g^b$ .

The partonic structure functions  $D_a^b$  satisfy an evolution equation which is best written when expressed in terms of the variables  $\ell$  and  $y$  and the functions  $\tilde{D}_a^b$  defined by [1] (see also (21) (23)):

$$x_b D_a^b(x_b, k_a, q) = \tilde{D}_a^b(\ell_b, y_b). \quad (44)$$

The parton content  $\tilde{D}_g$  of a gluon is shown in [6] to satisfy the evolution equation ( $Y$  and  $y$  are linked by (6))

$$\tilde{D}_g(\ell, y) = \delta(\ell) + \int_0^y dy' \int_0^\ell d\ell' \gamma_0^2(\ell' + y') [1 - a\delta(\ell' - \ell)] \tilde{D}_g(\ell', y'), \quad (45)$$

where the anomalous dimension  $\gamma_0(y)$  is given by ( $\lambda$  is defined in (39))

$$\gamma_0^2(y) = 4N_c \frac{\alpha_s(k_\perp^2)}{2\pi} \approx \frac{1}{\beta(y + \lambda)}. \quad (46)$$

(see the beginning of section 2 for  $\beta, T_R, C_F, \alpha_s, N_c$ ) and

$$a = \frac{1}{4N_c} \left[ \frac{11}{3}N_c + \frac{4}{3}T_R \left( 1 - \frac{2C_F}{N_c} \right) \right]; \quad C_F = 4/3 \text{ for } SU(3)_c. \quad (47)$$

The (single logarithmic) subtraction term proportional to  $a$  in (45) accounts for *gluon*  $\rightarrow$  *quark* transitions in parton cascades as well as for energy conservation – the so-called “hard corrections” to parton cascading –.

No superscript has been written in the structure functions  $D_g$  because the same equation is valid indifferently for  $D_g^g$  and  $D_g^q$  (see section 4). One considers that the same evolution equations govern the (inclusive) hadronic distributions  $D_g^h$  (Local Hadron Parton Duality).

In the small- $x$  approximation, the  $\delta(\ell)$  in (45) does not play any role.

#### A.2 Exact solution of the MLLA evolution equation for particle spectra

The exact solution of the evolution equation (45), which includes constraints of energy conservation and the running of  $\alpha_s$ , is demonstrated in [6] to be given by the following Mellin’s representation

$$\begin{aligned} \tilde{D}_g(\ell, y, \lambda) &= (\ell + y + \lambda) \int \frac{d\omega}{2\pi i} \int \frac{d\nu}{2\pi i} e^{\omega\ell + \nu y} \\ &\int_0^\infty \frac{ds}{\nu + s} \left( \frac{\omega(\nu + s)}{(\omega + s)\nu} \right)^{1/(\beta(\omega - \nu))} \left( \frac{\nu}{\nu + s} \right)^{a/\beta} e^{-\lambda s}. \end{aligned} \quad (48)$$

From (48) and taking the high energy limit  $\ell + y \equiv Y \gg \lambda^8$  one gets [1][15] the explicit formula

$$\tilde{D}_g(\ell, y) = \frac{\ell + y}{\beta B(B+1)} \int \frac{d\omega}{2\pi i} e^{-\omega y} \Phi(A+1, B+2, \omega(\ell + y)), \quad (49)$$

where  $\Phi$  is the confluent hypergeometric function the integral representation of which reads [16] [17]

$$\Phi(A+1, B+2, \omega Y) = \Gamma(B+2) (\omega Y)^{-B-1} \int \frac{dt}{(2\pi i)} \frac{t^{-B}}{t(t-1)} \left(\frac{t}{t-1}\right)^A e^{\omega Y t};$$

with  $A = \frac{1}{\beta\omega}$ ,  $B = \frac{a}{\beta}$ ,  $\Gamma(n) = \int_0^\infty d\chi \chi^{n-1} e^{-\chi}$ . (50)

Exchanging the  $t$  and  $\omega$  integrations of (49) (50) and going from  $t$  to the new variable  $\alpha = \frac{1}{2} \ln \frac{t}{t-1}$ , (49) becomes

$$\tilde{D}_g(\ell, y) = 2 \frac{\Gamma(B)}{\beta} \Re \left( \int_0^{\frac{\pi}{2}} \frac{d\tau}{\pi} e^{-B\alpha} \mathcal{F}_B(\tau, y, \ell) \right), \quad (51)$$

where the integration is performed with respect to  $\tau$  defined by  $\alpha = \frac{1}{2} \ln \frac{y}{\ell} + i\tau$ ,

$$\mathcal{F}_B(\tau, y, \ell) = \left[ \frac{\cosh \alpha - \frac{y-\ell}{y+\ell} \sinh \alpha}{\frac{\ell+y}{\beta} \frac{\alpha}{\sinh \alpha}} \right]^{B/2} I_B(2\sqrt{Z(\tau, y, \ell)}),$$

$$Z(\tau, y, \ell) = \frac{\ell+y}{\beta} \frac{\alpha}{\sinh \alpha} \left( \cosh \alpha - \frac{y-\ell}{y+\ell} \sinh \alpha \right); \quad (52)$$

$I_B$  is the modified Bessel function of the first kind.

### A.3 The spectrum

On Fig. 11 below, we represent, on the left, the spectrum as a function of the transverse momentum (via  $y$ ) for fixed  $\ell$  and, on the right, as a function of the energy (via  $\ell$ ) for fixed transverse momentum.

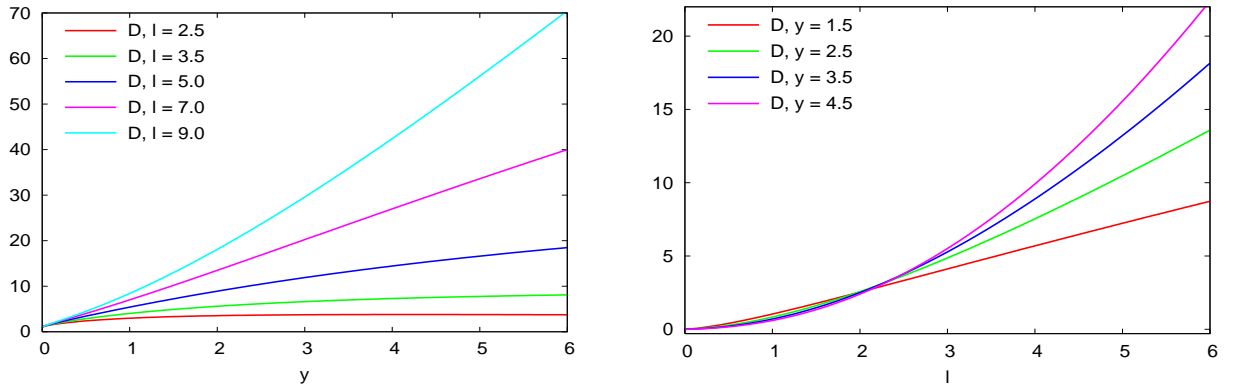


Fig. 11: spectrum  $\tilde{D}(\ell, y)$  of emitted partons as functions of transverse momentum (left) and energy (right)

<sup>8</sup> $Y \gg \lambda \Leftrightarrow E\Theta \gg Q_0^2/\Lambda_{QCD}$  is not strictly equivalent to  $Q_0 \rightarrow \Lambda_{QCD}$  (limiting spectrum).

Fig. 12 shows enlargements of Fig. 11 for small values of  $y$  and  $\ell$  respectively; they ease the understanding of the curves for the derivatives of the spectrum presented in subsection A.4.

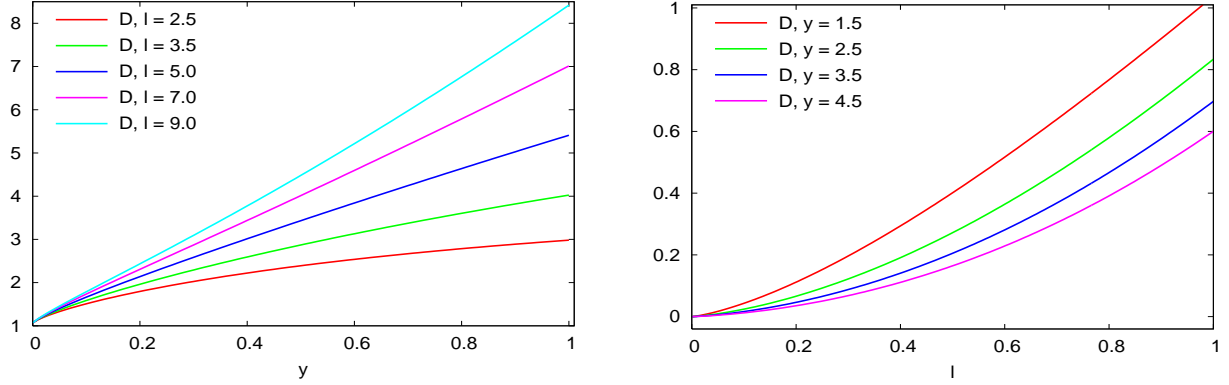


Fig. 12: spectrum  $\tilde{D}(\ell, y)$  of emitted partons as functions of transverse momentum (left) and energy (right): enlargement of Fig. 11

A comparison between MLLA and DLA calculations of the spectrum is done in appendix E.1.

#### A.4 Derivatives of the spectrum

We evaluate below the derivatives of the spectrum w.r.t.  $\ln k_{\perp}$  and  $\ln(1/x)$ .

We make use of the following property for the confluent hypergeometric functions  $\Phi$  [17]:

$$\frac{d}{d\ell}\Phi(A+1, B+2, \omega(\ell+y)) \equiv \frac{d}{dy}\Phi(A+1, B+2, \omega(\ell+y)) = \omega \frac{A+1}{B+2}\Phi(A+2, B+3, \omega(\ell+y)). \quad (53)$$

- We first determine the derivative w.r.t.  $\ell \equiv \ln(1/x)$ . Differentiating (49) w.r.t.  $\ell$ , and developing (53), one gets<sup>9</sup> [6]

$$\frac{d}{d\ell}\tilde{D}_g(\ell, y) = 2\frac{\Gamma(B)}{\beta} \int_0^{\frac{\pi}{2}} \frac{d\tau}{\pi} e^{-B\alpha} \left[ \frac{1}{\ell+y} (1 + 2e^{\alpha} \sinh \alpha) \mathcal{F}_B + \frac{1}{\beta} e^{\alpha} \mathcal{F}_{B+1} \right]; \quad (54)$$

- Differentiating w.r.t.  $y \equiv \ln \frac{k_{\perp}}{Q_0}$  yields

$$\frac{d}{dy}\tilde{D}_g(\ell, y) = 2\frac{\Gamma(B)}{\beta} \int_0^{\frac{\pi}{2}} \frac{d\tau}{\pi} e^{-B\alpha} \left[ \frac{1}{\ell+y} (1 + 2e^{\alpha} \sinh \alpha) \mathcal{F}_B + \frac{1}{\beta} e^{\alpha} \mathcal{F}_{B+1} - \frac{2 \sinh \alpha}{\ell+y} \mathcal{F}_{B-1} \right]. \quad (55)$$

In Fig. 13, Fig. 14, Fig. 15 and Fig. 16 below, we draw the curves for:

\*  $\frac{d\tilde{D}_g(\ell, y)}{dy}$  as a function of  $y$ , for different values of  $\ell$  fixed;

\*  $\frac{d\tilde{D}_g(\ell, y)}{d\ell}$  as a function of  $\ell$ , for different values of  $y$  fixed;

<sup>9</sup>(54) and (55) have also been checked by numerically differentiating (51).

- \*  $\frac{d\tilde{D}_g(\ell, y)}{d\ell}$  as a function of  $\ell$  for different values of  $y$  fixed;
- \*  $\frac{d\tilde{D}_g(\ell, y)}{dy}$  as a function of  $y$  for different values of  $\ell$  fixed.

In each case the right figure is an enlargement, close to the origin of axes, of the left figure.

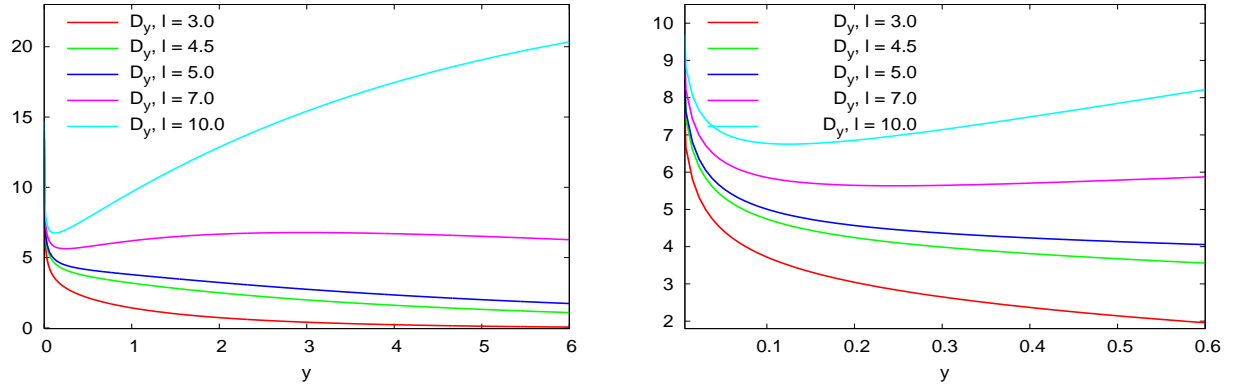


Fig. 13:  $\frac{d\tilde{D}_g(\ell, y)}{dy}$  as a function of  $y$  for different values of  $\ell$

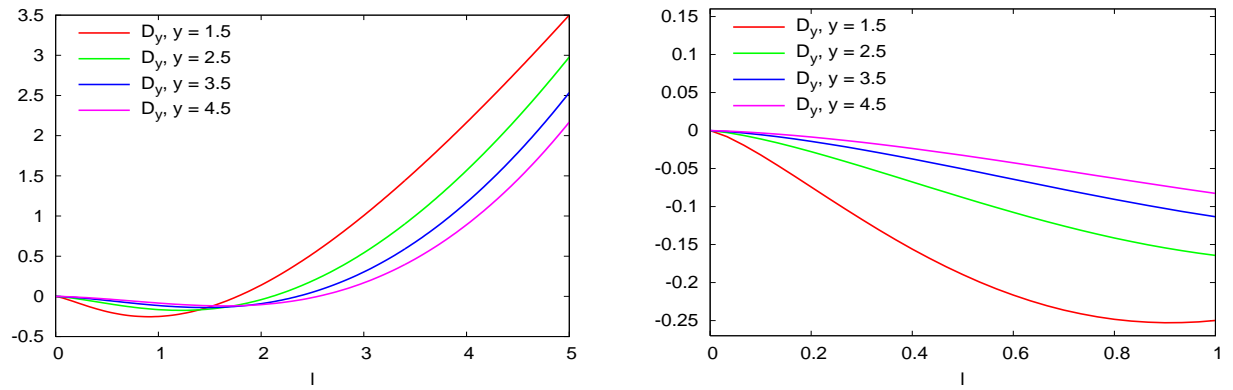


Fig. 14:  $\frac{d\tilde{D}_g(\ell, y)}{d\ell}$  as a function of  $\ell$  for different values of  $y$

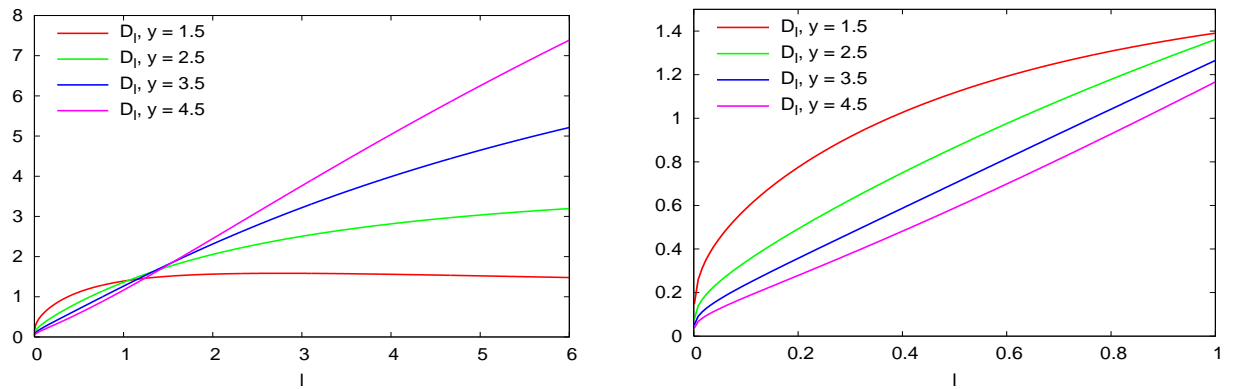


Fig. 15:  $\frac{d\tilde{D}_g(\ell, y)}{d\ell}$  as a function of  $\ell$  for different values of  $y$

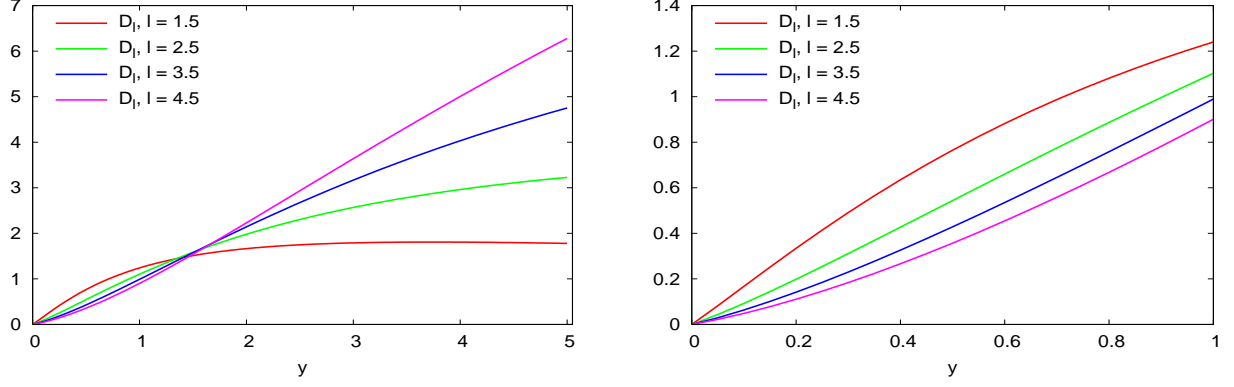


Fig. 16:  $\frac{d\tilde{D}_g(\ell, y)}{d\ell}$  as a function of  $y$  for different values of  $\ell$

That  $\frac{d\tilde{D}_g(\ell, y)}{dy}$  goes to infinity when  $y \rightarrow 0$  is in agreement with the analytic behavior in  $\ln(\ell/y)$  of this derivative.

## B LEADING CONTRIBUTIONS TO $x_1 F_{A_0}^{h_1}(x_1, \Theta, E, \Theta_0)$ AT SMALL $x_1$

Using (32), the leading terms of  $x_1 F_{A_0}^{h_1}(x_1, \Theta, E, \Theta_0)$  (26) calculated at small  $x_1$  read

$$\begin{aligned}
 x_1 F_g^{h_1}(x_1, \Theta, E, \Theta_0)^0 &\approx \tilde{D}_g(\ell_1, y_1) \left( \langle u \rangle_g^q + \frac{C_F}{N_c} \langle u \rangle_q^q \right) = \frac{\langle C \rangle_g^0}{N_c} \tilde{D}_g(\ell_1, y_1), \\
 x_1 F_q^{h_1}(x_1, \Theta, E, \Theta_0)^0 &\approx \tilde{D}_g(\ell_1, y_1) \left( \langle u \rangle_q^q + \frac{C_F}{N_c} \langle u \rangle_q^q \right) = \frac{\langle C \rangle_q^0}{N_c} \tilde{D}_g(\ell_1, y_1).
 \end{aligned} \tag{56}$$

The leading  $\langle C \rangle_g^0$  and  $\langle C \rangle_q^0$  in (34) for a quark and a gluon jet are given respectively by (see [1], chapt. 9<sup>10</sup>)

$$\begin{aligned}
 \langle C \rangle_q^0 &= \langle C \rangle_\infty - c_1 (N_c - C_F) \left( \frac{\ln(E\Theta/\Lambda_{QCD})}{\ln(E\Theta_0/\Lambda_{QCD})} \right)^{(c_3/4N_c\beta)} \\
 &= \langle C \rangle_\infty - c_1 (N_c - C_F) \left( \frac{Y_\Theta + \lambda}{Y_{\Theta_0} + \lambda} \right)^{(c_3/4N_c\beta)},
 \end{aligned} \tag{57}$$

$$\begin{aligned}
 \langle C \rangle_g^0 &= \langle C \rangle_\infty + c_2 (N_c - C_F) \left( \frac{\ln(E\Theta/\Lambda_{QCD})}{\ln(E\Theta_0/\Lambda_{QCD})} \right)^{(c_3/4N_c\beta)} \\
 &= \langle C \rangle_\infty + c_2 (N_c - C_F) \left( \frac{Y_\Theta + \lambda}{Y_{\Theta_0} + \lambda} \right)^{(c_3/4N_c\beta)},
 \end{aligned} \tag{58}$$

<sup>10</sup>The coefficient  $\beta$ , omitted in the exponents of eqs. (9.12a), (9.12b), (9.12c) of [1] has been restored here. The factor  $4N_c$  is due to our normalization (see the beginning of section 2).

with

$$\begin{aligned} \langle C \rangle_\infty &= c_1 N_c + c_2 C_F, \\ c_1 &= \frac{8 C_F}{3 c_3}, \quad c_2 = 1 - c_1 = \frac{2 n_f}{3 c_3}, \quad c_3 = \frac{8}{3} C_F + \frac{2}{3} n_f; \end{aligned} \quad (59)$$

in the r.h.s of (57) (58) we have used the definitions (6) (7).

In practice, we take in this work

$$Q_0 \approx \Lambda_{QCD} \Leftrightarrow \lambda \approx 0, \quad (60)$$

which ensures in particular the consistency with the analytical calculation of the MLLA spectrum (appendix A), which can only be explicitly achieved in this limit.

## C CALCULATION OF $\delta \langle C \rangle_g$ and $\delta \langle C \rangle_q$ OF SECTION 4

### C.1 Explicit expressions for $\langle u \rangle_{A_0}^A$ and $\delta \langle u \rangle_{A_0}^A$ defined in (28)

The expressions (28) for  $\langle u \rangle_{A_0}^A$  and  $\delta \langle u \rangle_{A_0}^A$  are conveniently obtained from the Mellin-transformed DGLAP fragmentation functions [1]

$$\mathcal{D}(j, \xi) = \int_0^1 du u^{j-1} D(u, \xi), \quad (61)$$

which, if one deals with  $D_A^B(u, r^2, s^2)$  depends in reality on the difference  $\xi(r^2) - \xi(s^2)$ :

$$\xi(Q^2) = \int_{\mu^2}^{Q^2} \frac{dk^2}{k^2} \frac{\alpha_s(k^2)}{4\pi}, \quad \xi(r^2) - \xi(s^2) \approx \frac{1}{4N_c\beta} \ln \left( \frac{\ln(r^2/\Lambda_{QCD}^2)}{\ln(s^2/\Lambda_{QCD}^2)} \right). \quad (62)$$

One has accordingly

$$\langle u \rangle_{A_0}^A = \mathcal{D}_{A_0}^A(2, \xi(E\Theta_0) - \xi(E\Theta)), \quad \delta \langle u \rangle_{A_0}^A = \frac{d}{dj} \mathcal{D}_{A_0}^A(j, \xi(E\Theta_0) - \xi(E\Theta)) \Big|_{j=2}. \quad (63)$$

The DGLAP functions  $\mathcal{D}(j, \xi)$  are expressed [1] in terms of the anomalous dimensions  $\nu_F(j)$ ,  $\nu_G(j)$  and  $\nu_\pm(j)$ , the  $j$  dependence of which is in particular known.

For the sake of completeness, we give below the expressions for the  $\langle u \rangle$ 's and  $\delta \langle u \rangle$ 's.

$$\begin{aligned} \langle u \rangle_g^q &= \frac{9}{25} \left( \left( \frac{Y_{\Theta_0} + \lambda}{Y_\Theta + \lambda} \right)^{\frac{50}{81}} - 1 \right) \left( \frac{Y_{\Theta_0} + \lambda}{Y_\Theta + \lambda} \right)^{-\frac{50}{81}}, \\ \langle u \rangle_g^g &= 1/25 \left( 16 \left( \frac{Y_{\Theta_0} + \lambda}{Y_\Theta + \lambda} \right)^{\frac{50}{81}} + 9 \right) \left( \frac{Y_{\Theta_0} + \lambda}{Y_\Theta + \lambda} \right)^{-\frac{50}{81}}, \end{aligned}$$



$$\begin{aligned}
\langle u \rangle_q^g &= \frac{16}{25} \left( \left( \frac{Y_{\Theta_0} + \lambda}{Y_{\Theta} + \lambda} \right)^{\frac{50}{81}} - 1 \right) \left( \frac{Y_{\Theta_0} + \lambda}{Y_{\Theta} + \lambda} \right)^{-\frac{50}{81}}, \\
\langle u \rangle_q^{sea} &= -1/25 \left( -9 \left( \frac{Y_{\Theta_0} + \lambda}{Y_{\Theta} + \lambda} \right)^{\frac{50}{81}} - 16 + 25 \left( \frac{Y_{\Theta_0} + \lambda}{Y_{\Theta} + \lambda} \right)^{2/9} \right) \left( \frac{Y_{\Theta_0} + \lambda}{Y_{\Theta} + \lambda} \right)^{-\frac{50}{81}}, \\
\langle u \rangle^{val} &= \left( \frac{Y_{\Theta_0} + \lambda}{Y_{\Theta} + \lambda} \right)^{-\frac{32}{81}}, \\
\langle u \rangle_q^{sea} + \langle u \rangle^{val} &= 1/25 \left( 9 \left( \frac{Y_{\Theta_0} + \lambda}{Y_{\Theta} + \lambda} \right)^{\frac{50}{81}} + 16 \right) \left( \frac{Y_{\Theta_0} + \lambda}{Y_{\Theta} + \lambda} \right)^{-\frac{50}{81}}; \\
\delta \langle u \rangle_q^g &= -\frac{1}{337500} \left( -43011 \left( \frac{Y_{\Theta_0} + \lambda}{Y_{\Theta} + \lambda} \right)^{\frac{50}{81}} + 43011 - 6804 \pi^2 \left( \frac{Y_{\Theta_0} + \lambda}{Y_{\Theta} + \lambda} \right)^{\frac{50}{81}} \right. \\
&\quad + 6804 \pi^2 - 48600 \ln \left( \frac{Y_{\Theta_0} + \lambda}{Y_{\Theta} + \lambda} \right) \left( \frac{Y_{\Theta_0} + \lambda}{Y_{\Theta} + \lambda} \right)^{\frac{50}{81}} \\
&\quad + 21600 \ln \left( \frac{Y_{\Theta_0} + \lambda}{Y_{\Theta} + \lambda} \right) \left( \frac{Y_{\Theta_0} + \lambda}{Y_{\Theta} + \lambda} \right)^{\frac{50}{81}} \pi^2 + 109525 \ln \left( \frac{Y_{\Theta_0} + \lambda}{Y_{\Theta} + \lambda} \right) \\
&\quad \left. - 17400 \ln \left( \frac{Y_{\Theta_0} + \lambda}{Y_{\Theta} + \lambda} \right) \pi^2 \right) \left( \frac{Y_{\Theta_0} + \lambda}{Y_{\Theta} + \lambda} \right)^{-\frac{50}{81}}, \\
\delta \langle u \rangle_q^g &= -\frac{1}{337500} \left( -11664 \left( \frac{Y_{\Theta_0} + \lambda}{Y_{\Theta} + \lambda} \right)^{\frac{50}{81}} + 31104 \pi^2 \left( \frac{Y_{\Theta_0} + \lambda}{Y_{\Theta} + \lambda} \right)^{\frac{50}{81}} \right. \\
&\quad - 86400 \ln \left( \frac{Y_{\Theta_0} + \lambda}{Y_{\Theta} + \lambda} \right) \left( \frac{Y_{\Theta_0} + \lambda}{Y_{\Theta} + \lambda} \right)^{\frac{50}{81}} \\
&\quad + 38400 \ln \left( \frac{Y_{\Theta_0} + \lambda}{Y_{\Theta} + \lambda} \right) \left( \frac{Y_{\Theta_0} + \lambda}{Y_{\Theta} + \lambda} \right)^{\frac{50}{81}} \pi^2 \\
&\quad + 11664 - 31104 \pi^2 - 109525 \ln \left( \frac{Y_{\Theta_0} + \lambda}{Y_{\Theta} + \lambda} \right) \\
&\quad \left. + 17400 \ln \left( \frac{Y_{\Theta_0} + \lambda}{Y_{\Theta} + \lambda} \right) \pi^2 \right) \left( \frac{Y_{\Theta_0} + \lambda}{Y_{\Theta} + \lambda} \right)^{-\frac{50}{81}}, \\
\delta \langle u \rangle_q^g &= -\frac{4}{759375} \left( 48114 \left( \frac{Y_{\Theta_0} + \lambda}{Y_{\Theta} + \lambda} \right)^{\frac{50}{81}} - 48114 - 6804 \pi^2 \left( \frac{Y_{\Theta_0} + \lambda}{Y_{\Theta} + \lambda} \right)^{\frac{50}{81}} \right. \\
&\quad + 6804 \pi^2 - 48600 \ln \left( \frac{Y_{\Theta_0} + \lambda}{Y_{\Theta} + \lambda} \right) \left( \frac{Y_{\Theta_0} + \lambda}{Y_{\Theta} + \lambda} \right)^{\frac{50}{81}} \\
&\quad + 21600 \ln \left( \frac{Y_{\Theta_0} + \lambda}{Y_{\Theta} + \lambda} \right) \left( \frac{Y_{\Theta_0} + \lambda}{Y_{\Theta} + \lambda} \right)^{\frac{50}{81}} \pi^2 + 109525 \ln \left( \frac{Y_{\Theta_0} + \lambda}{Y_{\Theta} + \lambda} \right) \\
&\quad \left. - 17400 \ln \left( \frac{Y_{\Theta_0} + \lambda}{Y_{\Theta} + \lambda} \right) \pi^2 \right) \left( \frac{Y_{\Theta_0} + \lambda}{Y_{\Theta} + \lambda} \right)^{-\frac{50}{81}},
\end{aligned}$$

$$\begin{aligned}
\delta \langle u \rangle_q^{sea} &= \frac{2}{759375} \left( -13122 \left( \frac{Y_{\Theta_0} + \lambda}{Y_{\Theta} + \lambda} \right)^{\frac{50}{81}} + 34992 \pi^2 \left( \frac{Y_{\Theta_0} + \lambda}{Y_{\Theta} + \lambda} \right)^{\frac{50}{81}} \right. \\
&\quad + 54675 \ln \left( \frac{Y_{\Theta_0} + \lambda}{Y_{\Theta} + \lambda} \right) \left( \frac{Y_{\Theta_0} + \lambda}{Y_{\Theta} + \lambda} \right)^{\frac{50}{81}} \\
&\quad - 24300 \ln \left( \frac{Y_{\Theta_0} + \lambda}{Y_{\Theta} + \lambda} \right) \left( \frac{Y_{\Theta_0} + \lambda}{Y_{\Theta} + \lambda} \right)^{\frac{50}{81}} \pi^2 \\
&\quad + 13122 - 34992 \pi^2 + 219050 \ln \left( \frac{Y_{\Theta_0} + \lambda}{Y_{\Theta} + \lambda} \right) - 34800 \ln \left( \frac{Y_{\Theta_0} + \lambda}{Y_{\Theta} + \lambda} \right) \pi^2 \\
&\quad - 265625 \ln \left( \frac{Y_{\Theta_0} + \lambda}{Y_{\Theta} + \lambda} \right) \left( \frac{Y_{\Theta_0} + \lambda}{Y_{\Theta} + \lambda} \right)^{\frac{2}{9}} \\
&\quad \left. + 37500 \ln \left( \frac{Y_{\Theta_0} + \lambda}{Y_{\Theta} + \lambda} \right) \left( \frac{Y_{\Theta_0} + \lambda}{Y_{\Theta} + \lambda} \right)^{\frac{2}{9}} \pi^2 \right) \left( \frac{Y_{\Theta_0} + \lambda}{Y_{\Theta} + \lambda} \right)^{-\frac{50}{81}},
\end{aligned}$$

$$\delta \langle u \rangle^{val} = -\frac{2}{243} (-85 + 12 \pi^2) \ln \left( \frac{Y_{\Theta_0} + \lambda}{Y_{\Theta} + \lambda} \right) \left( \frac{Y_{\Theta_0} + \lambda}{Y_{\Theta} + \lambda} \right)^{-\frac{32}{81}},$$

$$\begin{aligned}
\delta \langle u \rangle^{val} + \delta \langle u \rangle_q^{sea} &= -\frac{2}{759375} \left( 13122 \left( \frac{Y_{\Theta_0} + \lambda}{Y_{\Theta} + \lambda} \right)^{\frac{50}{81}} - 34992 \pi^2 \left( \frac{Y_{\Theta_0} + \lambda}{Y_{\Theta} + \lambda} \right)^{\frac{50}{81}} \right. \\
&\quad - 54675 \ln \left( \frac{Y_{\Theta_0} + \lambda}{Y_{\Theta} + \lambda} \right) \left( \frac{Y_{\Theta_0} + \lambda}{Y_{\Theta} + \lambda} \right)^{\frac{50}{81}} \\
&\quad + 24300 \ln \left( \frac{Y_{\Theta_0} + \lambda}{Y_{\Theta} + \lambda} \right) \left( \frac{Y_{\Theta_0} + \lambda}{Y_{\Theta} + \lambda} \right)^{\frac{50}{81}} \pi^2 - 13122 + 34992 \pi^2 \\
&\quad \left. - 219050 \ln \left( \frac{Y_{\Theta_0} + \lambda}{Y_{\Theta} + \lambda} \right) + 34800 \ln \left( \frac{Y_{\Theta_0} + \lambda}{Y_{\Theta} + \lambda} \right) \pi^2 \right) \left( \frac{Y_{\Theta_0} + \lambda}{Y_{\Theta} + \lambda} \right)^{-\frac{50}{81}}.
\end{aligned} \tag{64}$$

When  $\Theta \rightarrow \Theta_0$ , all  $\delta \langle u \rangle$ 's vanish, ensuring that the limits  $\xi(E\Theta_0) - \xi(E\Theta) \rightarrow 0$  of the  $\langle C \rangle_{A_0}^0 + \delta \langle C \rangle_{A_0}$ 's are the same as the ones of the  $\langle C \rangle_{A_0}^0$ 's.

## C.2 $\delta \langle C \rangle_q$ and $\delta \langle C \rangle_g$

They are given in (35), and one uses (32) such that only  $\psi_{g,\ell_1}$  (see (29)) appears. Their full analytical expressions for the  $\delta \langle C \rangle$ 's are too complicated to be easily written and manipulated.

Using the formulæ of C.1, one gets the approximate results

$$\begin{aligned}
\delta \langle C \rangle_q &\approx \left( 1.4676 - 1.4676 \left( \frac{Y_{\Theta_0} + \lambda}{Y_{\Theta} + \lambda} \right)^{-\frac{50}{81}} - 3.2510 \ln \left( \frac{Y_{\Theta_0} + \lambda}{Y_{\Theta} + \lambda} \right) \right. \\
&\quad \left. + 0.5461 \left( \frac{Y_{\Theta_0} + \lambda}{Y_{\Theta} + \lambda} \right)^{-\frac{50}{81}} \ln \left( \frac{Y_{\Theta_0} + \lambda}{Y_{\Theta} + \lambda} \right) \right) \psi_{g,\ell_1}(\ell_1, y_1), \tag{65}
\end{aligned}$$

and

$$\delta \langle C \rangle_g \approx \left( -2.1898 + 2.1898 \left( \frac{Y_{\Theta_0} + \lambda}{Y_{\Theta} + \lambda} \right)^{-\frac{50}{81}} - 3.2510 \ln \left( \frac{Y_{\Theta_0} + \lambda}{Y_{\Theta} + \lambda} \right) \right)$$

$$-0.3072 \left( \frac{Y_{\Theta_0} + \lambda}{Y_{\Theta} + \lambda} \right)^{-\frac{50}{81}} \ln \left( \frac{Y_{\Theta_0} + \lambda}{Y_{\Theta} + \lambda} \right) \psi_{g,\ell_1}(\ell_1, y_1). \quad (66)$$

The logarithmic derivative  $\psi_{g,\ell_1}(\ell_1, y_1)$  (29) of the MLLA spectrum  $\tilde{D}_g(\ell_1, y_1)$  is obtained from (51) of appendix A.

## D THE AVERAGE COLOR CURRENT $\langle C \rangle_{A_0}$

On Fig. 17 below, we plot, for  $Y_{\Theta_0} = 7.5$ ,  $\langle C \rangle_q^0$ ,  $\langle C \rangle_q^0 + \delta \langle C \rangle_q$ ,  $\langle C \rangle_g^0$ ,  $\langle C \rangle_g^0 + \delta \langle C \rangle_g$  as functions of  $y$ , for  $\ell = 2.5$  on the left and  $\ell = 3.5$  on the right. Since  $\Theta \leq \Theta_0$ , the curves stop at  $y$  such that  $y + \ell = \Theta_0$ ; they reach then their respective asymptotic values  $N_c$  for  $\langle C \rangle_g$  and  $C_F$  for  $\langle C \rangle_q$ , at which  $\delta \langle C \rangle_q$  and  $\delta \langle C \rangle_g$  also vanish (see also the naive approach (38)). These corrections also vanish at  $y = 0$  because they are proportional to the logarithmic derivative  $(1/\tilde{D}(\ell, y))(d\tilde{D}(\ell, y)/dy)$  (see (35)) which both vanish, for  $q$  and  $g$ , at  $y = 0$  (see appendix A, and Figs. 15-16).

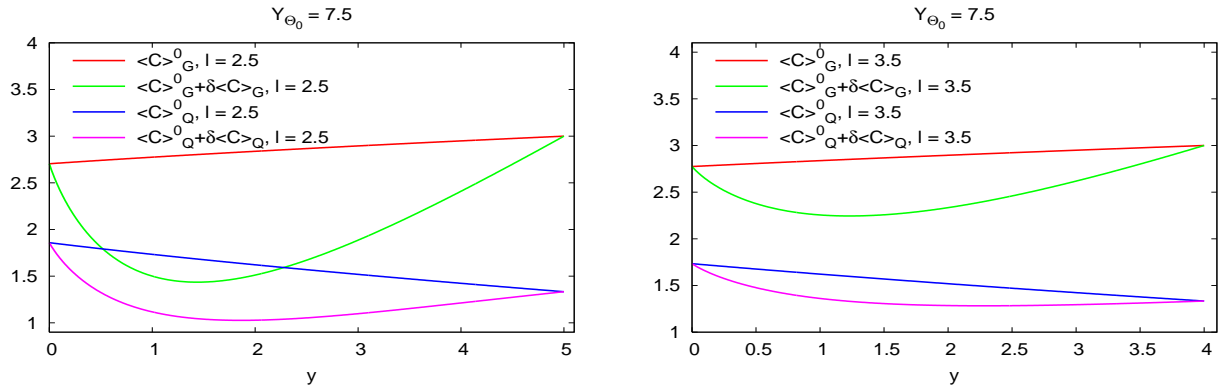


Fig. 17:  $\langle C \rangle_{A_0}^0$  and  $\langle C \rangle_{A_0}^0 + \delta \langle C \rangle_{A_0}$  for quark and gluon jets, as functions of  $y$ , for  $Y_{\Theta_0} = 7.5$ ,  $\ell = 2.5$  on the left and  $\ell = 3.5$  on the right.

## E COMPARING DLA AND MLLA APPROXIMATIONS

DLA [11] [12] and MLLA approximations are very different [1]; in particular, the exact balance of energy (recoil effects of partons) is not accounted for in DLA.

We compare DLA and MLLA results for the two distributions of concern in this work. Studying first their difference for the spectrum itself eases the rest of the comparison.

We choose the two values  $Y_{\Theta_0} = 7.5$  and  $Y_{\Theta_0} = 15$ . While the first corresponds to the LHC working conditions, the second is purely academic since, taking for example  $\Theta_0 \approx .5$  and  $Q_0 \approx 250 \text{ MeV}$ , it corresponds to an energy of  $1635 \text{ TeV}$ ; it is however suitable, as we shall see in subsection E.3 to disentangle the effects of coherence and the ones of the divergence of  $\alpha_s$  at low energy in the calculation of the inclusive  $k_{\perp}$  distribution.

## E.1 The spectrum

Fixing  $\alpha_s$  in DLA at the largest scale of the process, the collision energy, enormously damps the corresponding spectrum (it does not take into account the growing of  $\alpha_s$  accompanying parton cascading), which gives an unrealistic aspect to the comparison.

This is why, as far as the spectra are concerned, we shall compare their MLLA evaluation with that obtained from the latter by taking to zero the coefficient  $a$  given in (47), which also entails  $B = 0$ ;  $\mathcal{F}_0(\tau, y, \ell)$  in (52) becomes  $I_0(2\sqrt{Z(\tau, y, \ell)})$ . The infinite normalization that occurs in (51) because of  $\Gamma(B = 0)$  we replace by a constant such that the two calculations can be easily compared. This realizes a DLA approximation (no accounting for recoil effects) “with running  $\alpha_s$ ”.

On Fig. 18 below are plotted the spectrum  $\tilde{D}_g(\ell, y \equiv Y_{\Theta_0} - \ell)$  for gluon jets in the MLLA and DLA “with running  $\alpha_s$ ” approximations.

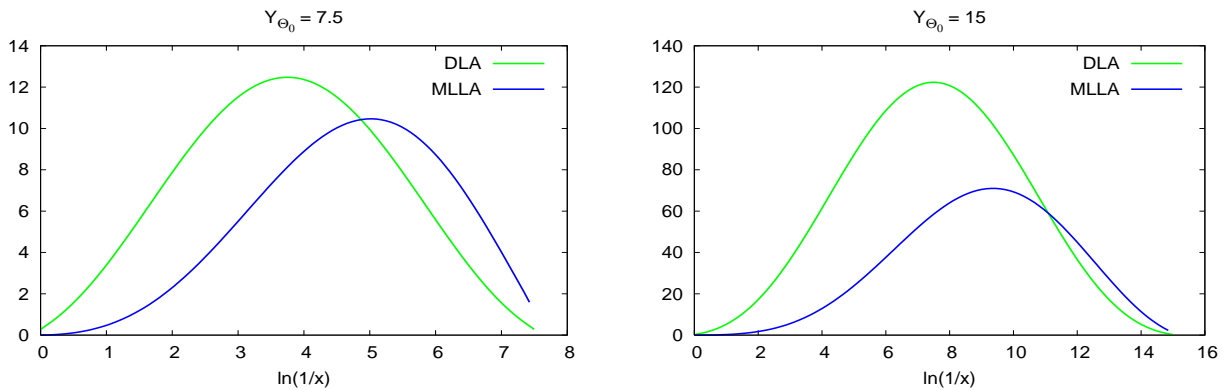


Fig. 18: the spectrum  $\tilde{D}_g(\ell, Y_{\Theta_0} - \ell)$  for gluon jets; comparison between MLLA and DLA (“with running  $\alpha_s$ ”) calculations.

The peak of the MLLA spectrum is seen, as expected, to occur at smaller values of the energy than that of DLA.

## E.2 Double differential 1-particle inclusive distribution

The genuine MLLA calculations being already shown on Figs. 2 and 4, Fig. 19 displays, on the left, a “modified” MLLA calculation obtained by dividing by  $\alpha_s(k_{\perp}^2) \approx \frac{\pi}{2N_c\beta y}$  (see (46) with  $\lambda \rightarrow 0$ ); subtracting in the MLLA calculations the dependence on  $k_{\perp}$  due to the running of  $\alpha_s(k_{\perp}^2)$  allows a better comparison with DLA (with fixed  $\alpha_s$ ) by getting rid of the divergence when  $k_{\perp} \rightarrow Q_0$ .

On the right are plotted the DLA results for gluon jets, in which  $\alpha_s$  has been fixed at the collision energy (it is thus very small). Since their normalizations are now different, only the *shapes* of the two types of curves must be compared; we indeed observe that the DLA growing of  $\frac{d^2N}{d\ell_1 d\ln k_{\perp}}$  with  $k_{\perp}$  (or  $y_1$ ) also occurs in the “modified” MLLA curves.

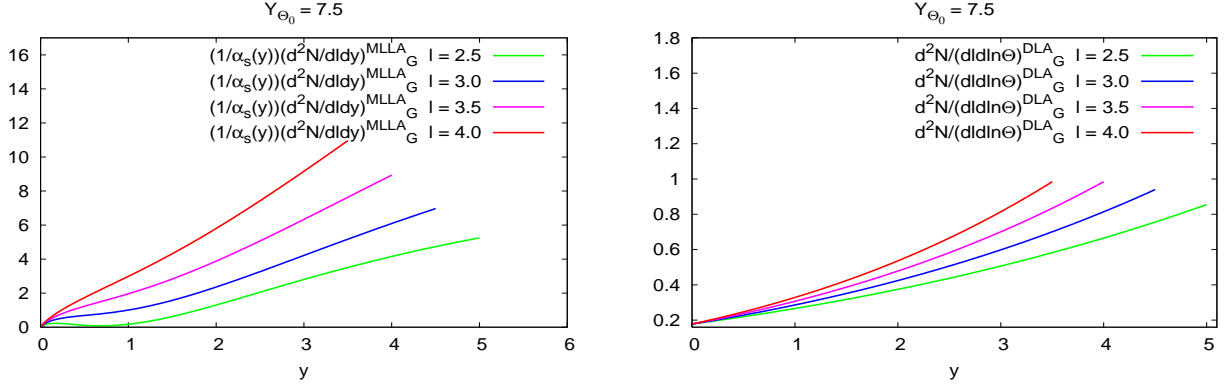


Fig. 19: comparison between MLLA (after dividing by  $\alpha_s(k_\perp^2)$ , on the left) and DLA calculation with  $\alpha_s$  fixed (on the right) of  $\frac{d^2 N}{dy d \ln k_\perp}$  for gluon jets.

The DLA distribution for quark jets is obtained from that of gluon jets by multiplication by the factor  $C_F/N_c$ ; it is thus also a growing function of  $y_1$ .

The MLLA distribution for quark jets, which is, unlike that for gluon jets, a decreasing function of  $y_1$  (see Fig. 5), becomes, like the latter, growing, after the dependence on  $\alpha_s(k_\perp^2)$  has been divided out: one finds the same behavior as in DLA.

### E.3 Inclusive $k_\perp$ distribution

On Fig. 20 we have plotted, at  $Y_{\theta_0} = 7.5$ :

- the MLLA calculation of  $\frac{dN}{d \ln k_\perp}$  divided by  $\alpha_s(k_\perp^2)$ , such that the divergence due to the running of  $\alpha_s$  has been divided out, leaving unperturbed the damping due to coherence effects;
- the DLA calculation of  $\frac{dN}{d \ln k_\perp}$  with  $\alpha_s$  fixed at the collision energy.

Like in E.2, because of the division by  $\alpha_s$ , the two curves are not normalized alike, such that only their *shapes* should be compared.

The comparison of the DLA curve (at fixed  $\alpha_s$ ) with the genuine MLLA calculation displayed in Fig. 6 (left) shows how different are the outputs of the two approximations; while at large  $k_\perp$  they are both decreasing, at small  $k_\perp$  the running of  $\alpha_s$  makes the sole MLLA distribution diverge when  $k_\perp \rightarrow Q_0$  (non-perturbative domain).

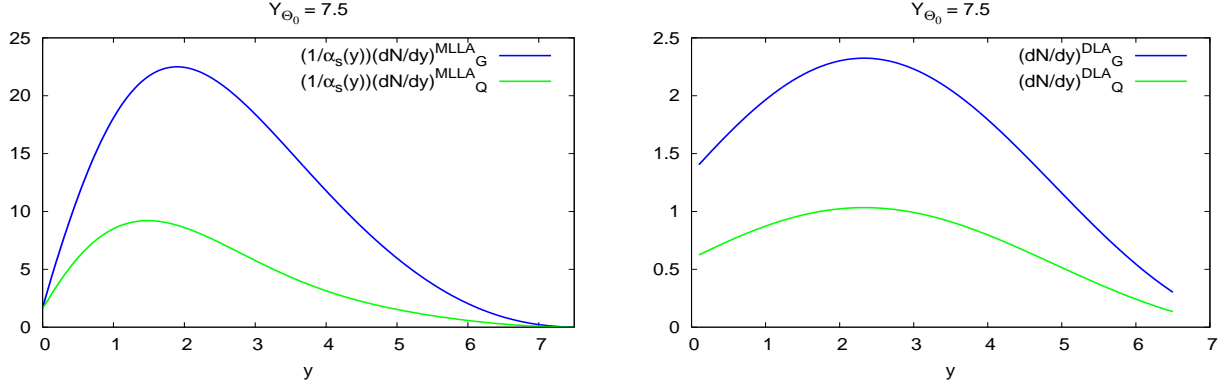


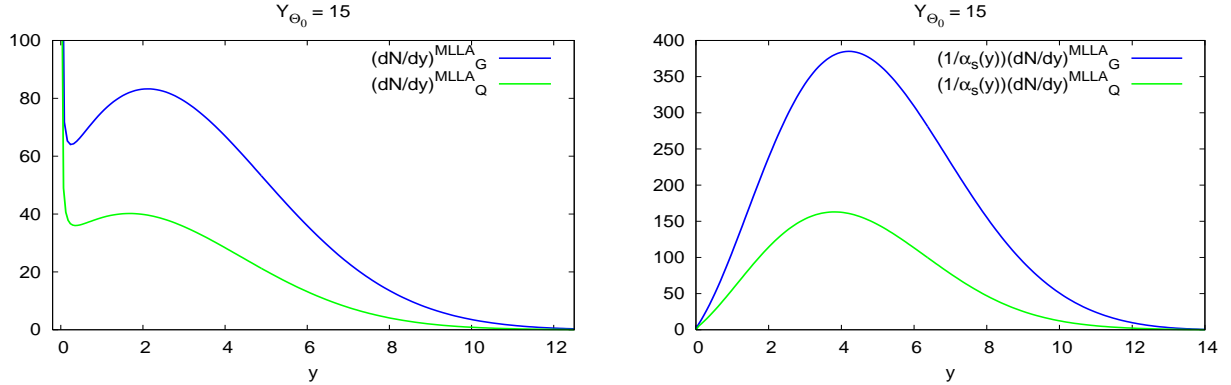
Fig. 20:  $Y_{\Theta_0} = 7.5$ : comparing MLLA and DLA calculations of  $\frac{dN}{d \ln k_{\perp}}$  (see also Fig. 6); from left to right:  $\frac{1}{\alpha_s(k_{\perp}^2)}$  MLLA and DLA ( $\alpha_s$  fixed).

In the extremely high domain of energy  $Y_{\Theta_0} = 15$  used for Fig. 21, the two competing phenomena occurring at small  $y_1$  can then be neatly distinguished.

The first plot, showing MLLA results, cleanly separates coherence effects from the running of  $\alpha_s$ ; in the second figure we have plotted the MLLA calculation divided by  $\alpha_s(k_{\perp}^2)$ : damping at small  $y_1$  due to coherence effects appears now unspoiled; finally, DLA calculations clearly exhibit, too, the damping due to coherence<sup>11</sup>.

The large difference of magnitude observed between the first (genuine MLLA) and the last (DLA) plots occurs because DLA calculations have been performed with  $\alpha_s$  fixed at the very high collision energy.

Like in E.2, because of the division by  $\alpha_s$ , the second curve is not normalized like the two others, such that only its *shape* should be compared with theirs.



<sup>11</sup>The DLA points corresponding to  $y_1 = 0$  can be analytically determined to be  $4N_c/n_f$  (gluon jet) and  $4C_F/n_f$  (quark jet); they are independent of the energy  $Y_{\Theta_0}$ .

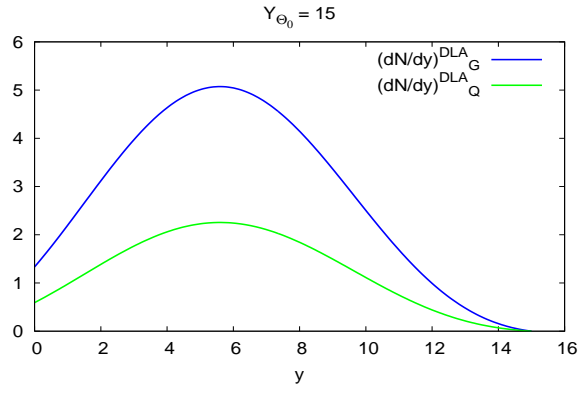


Fig. 21:  $Y_{\Theta_0} = 15$ : comparing MLLA and DLA calculations of  $\frac{dN}{d \ln k_{\perp}}$ ; from left to right: MLLA,  $\frac{1}{\alpha_s(k_T^2)}$ MLLA and DLA ( $\alpha_s$  fixed).

## Figure captions

Fig. 1: the process under consideration: two hadrons  $h_1$  and  $h_2$  inside one jet;

Fig. 2:  $\frac{d^2 N}{d\ell_1 d\ln k_\perp}$  for a gluon jet,  $Y_{\Theta_0} = 7.5$  and  $Y_{\Theta_0} = 10$ ;

Fig. 3:  $\frac{d^2 N}{d\ell_1 d\ln k_\perp}$  at fixed  $\ell_1$  for a gluon jet, comparison between MLLA and the naive approach;

Fig. 4:  $\frac{d^2 N}{d\ell_1 d\ln k_\perp}$  for a quark jet,  $Y_{\Theta_0} = 7.5$  and  $Y_{\Theta_0} = 10$ ;

Fig. 5:  $\frac{d^2 N}{d\ell_1 d\ln k_\perp}$  at fixed  $\ell_1$  for a quark jet, comparison between MLLA and the naive approach;

Fig. 6: inclusive  $k_\perp$  distribution  $\frac{dN}{d\ln k_\perp}$  for a gluon jet,  $Y_{\Theta_0} = 7.5$  and  $Y_{\Theta_0} = 10$ , MLLA and naive approach, both for  $\ell_{min} = 0$ ;

Fig. 7: enlargements of Fig. 6 at large  $k_\perp$ ;

Fig. 8: inclusive  $k_\perp$  distribution  $\frac{dN}{d\ln k_\perp}$  for a quark jet,  $Y_{\Theta_0} = 7.5$  and  $Y_{\Theta_0} = 10$ , MLLA and naive approach, both for  $\ell_{min} = 0$ ;

Fig. 9: enlargements of Fig. 8 at large  $k_\perp$ ;

Fig. 10: role of the upper limit of integration over  $x_1$  in the inclusive  $k_\perp$  distribution  $\frac{dN}{d\ln k_\perp}$  for gluon (left) and quark (right) jet;

Fig. 11: spectrum  $\tilde{D}_g(\ell, y)$  of emitted partons as functions of transverse momentum (left) and energy (right);

Fig. 12: enlargements of Fig. 11 close to the origin;

Fig. 13:  $\frac{d\tilde{D}_g(\ell, y)}{dy}$  as a function of  $y$  for different values of  $\ell$ ;

Fig. 14:  $\frac{d\tilde{D}_g(\ell, y)}{dy}$  as a function of  $\ell$  for different values of  $y$ ;

Fig. 15:  $\frac{d\tilde{D}_g(\ell, y)}{d\ell}$  as a function of  $\ell$  for different values of  $y$ ;

Fig. 16:  $\frac{d\tilde{D}_g(\ell, y)}{d\ell}$  as a function of  $y$  for different values of  $\ell$ ;

Fig. 17:  $\langle C \rangle_{A_0}^0$  and  $\langle C \rangle_{A_0}^0 + \delta \langle C \rangle_{A_0}$  for quark and gluon jets, as functions of  $y$ , for  $Y_{\Theta_0} = 7.5$ ,  $\ell = 2.5$  on the left and  $\ell = 3.5$  on the right;

Fig. 18: the spectrum  $\tilde{D}_g(\ell, Y_{\Theta_0} - \ell)$  for gluon jets; comparison between MLLA and DLA (“with running  $\alpha_s$ ”) calculations;

Fig. 19: comparison between MLLA (after dividing by  $\alpha_s(k_\perp^2)$ , on the left) and DLA calculation with  $\alpha_s$  fixed (on the right) of  $\frac{d^2 N}{dy d\ln k_\perp}$  for gluon jets;

Fig. 20:  $Y_{\Theta_0} = 7.5$ : comparing MLLA and DLA calculations of  $\frac{dN}{d\ln k_\perp}$  (see also Fig. 6); from left to right:  $\frac{1}{\alpha_s(k_T^2)}$ MLLA and DLA ( $\alpha_s$  fixed);

Fig. 21:  $Y_{\Theta_0} = 15$ : comparing MLLA and DLA calculations of  $\frac{dN}{d\ln k_\perp}$ ; from left to right: MLLA,  $\frac{1}{\alpha_s(k_T^2)}$ MLLA and DLA ( $\alpha_s$  fixed).



## References

- [1] Yu.L. Dokshitzer, V.A. Khoze, A.H. Mueller and S.I. Troyan: “*Basics of Perturbative QCD*” (Editions Frontières, Paris, 1991), and references therein.
- [2] C.P. Fong and B.R. Webber: Phys. Lett. **B 229** (1989) 289.
- [3] OPAL Collab., M.Z. Akrawy et al.: Phys. Lett. **B 247** (1990) 617-628.  
JADE Collab. and OPAL Collab., P. Pfeifenschneider et al.: Eur. Phys. J. **C 17** (2000) 19-51.
- [4] CDF Collab., T. Affolder et al.: Phys. Rev. Lett. **87** (2001) 211804;  
CDF Collab., D. Acosta et al.: Phys. Rev. **D 68** (2003) 012003.
- [5] H1 Collab., C. Adloff et al.: Eur. Phys. J. **C 21** (2001) 33-61;  
H1 Collab., C. Adloff et al.: Phys. Lett. **B 542** (2002) 193.
- [6] Yu.L. Dokshitzer and R. Perez Ramos: “*Two particle correlations in QCD jets*” , Sept. 2005, to appear.
- [7] Yu.L. Dokshitzer, D.I. Dyakonov and S.I. Troyan: “*Inelastic processes in Quantum Chromodynamics*”, SLAC-TRANS-183, translated from Proceedings of 13th Leningrad Winter School (1978), 1-89;  
Yu.L. Dokshitzer, D.I. Dyakonov and S.I. Troyan: “*Hard processes in Quantum Chromodynamics*”, Phys. Rept. **58** (1980) 269-395.
- [8] Yu.L. Dokshitzer and D.I. Dyakonov: “*Quantum Chromodynamics and hadron jets*”, DESY-L-TRANS-234 (Jul. 1979). Translated from Proceedings of 14th Leningrad Winter School (1979) p. 27-108 (translation).
- [9] H.D. Politzer: Phys. Rep. **14 C** (1974) 130.
- [10] V.N. Gribov and L.N. Lipatov: Sov. J. Nucl. Phys. **15** (1972) 438 and 675;  
L.N. Lipatov: Sov. J. Nucl. Phys. **20** (1975) 94;  
A.P. Bukhvostov, L.N. Lipatov and N.P. Popov: Sov. J. Nucl. Phys. **20** (1975) 286;  
G. Altarelli and G. Parisi: Nucl. Phys. **B 126** (1977) 298;  
Yu.L. Dokshitzer: Sov. Phys. JETP **46** (1977) 641.
- [11] Yu.L. Dokshitzer, V.S. Fadin and V.A. Khoze: Z. Phys. **C18** (1983) 37.
- [12] Yu.L. Dokshitzer, V.S. Fadin and V.A. Khoze: Phys. Lett. **B 115** (1982) 242.
- [13] Yu.L. Dokshitzer, V.A. Khoze, S.I. Troyan and A.H. Mueller: Rev. Mod. Phys. **60** (1988) 373-388.
- [14] R. Perez-Ramos & G.P. Salam: in preparation.
- [15] V.A. Khoze and W. Ochs: Int. J. Mod. Phys. **A12** (1997) 2949.
- [16] I.S. Gradshteyn and I.M. Ryzhik: “*Table of Integrals, Series, and Products*” (Academic Press, New York and London, 1965).
- [17] L.J. Slater, D. Lit (Ph.D): “*Confluent Hypergeometric Functions*”, Cambridge University Press (London, New-York) 1960.